



Applications of Spectral Relaxation Method on Nonlinear Ordinary Differential Equations Governing some types of fluid flow

تطبيقات طريقة الطيف المسترخية على المعادلات التفاضلية العادية اللاخطية التي تصف بعض أنواع سريان المائع

A thesis Submitted in Partial Fulfilment for the Degree of M.Sc in Mathematics

By

Limia Elmnsour Omer Elmnsour

Supervisor

Dr. Mohamed Hassan Mohamed Khabir

March 2016

الآیه
Abstract
Abstract (in Arabic) v
Dedication
Aknowledgments I
Chapter 1 1
Introduction
Chapter 2 3
2.1Spectral method
2.2 Spectral relaxation method
Chapter 3
3.1 Mathematical Formulation
3.2 Numerical solution 10
3.3 Results 11
Chapter 4 24
4.1 Mathematical Function
4.2 Numerical solution
4.3 Results
Chapter 5 42
Over all conclusions
References 43

بِسْمِ اللهِ الرَّحْمنِ الرَّحِيمِ

قال تعالى:

﴿ شَهِدَ اللَّهُ أَنَّهُ لاَ إِلَهَ إِلاَّ هُوَ وَالْمَلائِكَةُ وَأُولُواْ الْعِلْمِ قَائِمًا بِالْقِسْطِ لَا شَهِدَ اللَّهُ أَنَّهُ لاَ إِلَهَ إِلاَّ هُوَ الْعَزِيزُ الْحَكِيمِ ﴾ لاَ إِلَهَ إِلاَّ هُوَ الْعَزِيزُ الْحَكِيمِ ﴾

صدق الله العظيم سوره آل عمران ﴿١٨﴾

Abstract

In this thesis we solve systems of nonlinear ordinary differential equations by applying the spectral relaxation method (SRM). The SRM is an efficient numerical method that gives accurate results. First we give a historical idea and details of the SRM method. Then we present a study of a boundary layer flow with a convective surface boundary condition. The system of equations governing the thermo-hydrodynamic boundary layer flow is solved using the spectral relaxation method. The effects of the governing fluid parameters on the velocity, temperature and concentration profiles are also studied . Dufour and Soret effects on incompressible Newtonian fluid flow over a vertical down-pointing cone, are investigated studied numerically by using the spectral relaxation method. Results presented in this study are compared with those of previously published literature for selected values of the governing physical parameters. We also analysed the residual error and we investigate the accuracy of the method, and then we compare the result against solutions obtained from published literature.

الخلاصة

في هذا البحث قمنا بتطبيق طريقة الطيف المسترخية لحل أنواع مختلفة من المعادلات التفاضلية العادية اللاخطية. طريقة الطيف المسترخية هي طريقة عددية تعطي نتائج دقيقة. بداية اعطينا فكرة مفصلة عن طريقة الطيف المسترخية. ثم تطرقنا الي الإنسياب علي الطبقات الحدية مع شروط سطح الحمل الحراري الحدية. تم حل نظام المعادلات التي تصف إنسياب الطبقات الحدية الحرارية الهيدروديناميكية باستخدام طريقة الطيف المسترخية ايضا تم دراسة التأثيرات التي تصف وسائط المائع علي السرعة والحرارة والتركيز .تأثيرات دوفور وسيوريت علي إنسياب المائع النيوتوني الغير منضغط الذي يمر علي مخروط مقلوب القاعدة ،تم دراستها عدديا باستخدام طريقة الطيف المسترخية بمقارنة نتائجنا مع نتائج دراسات سابقة لبعض قيم الوسائط الفيزيائية المختارة. ايضا تحققنا من الخطأ المتبقى والدقة الجبرية.

Dedication

Mother & Father

The two persons that gave the tools and values necessary to be where I am standing today.

Beloved brothers, sister and my dear friends
To my Dr.Faiz.G.Awad for his guidance, help
and support, a good teachers like you are
few, you are loyal, always making learning
fun-filled, joyful, beneficial and memorable
experience for me ...you are creativity behind
our success.

Aknowledgments

All thanks to my God,

To my

Dr. Mohamed Hassan Mohamed Khabir&

Dr.Faiz.G.Awad

For advising, encouraging and helping me to finishing

This work.

Chapter 1

Overall introduction

The spectral relaxation method is a numerical technique based on simple iteration schemes formed by reducing large systems of nonlinear equations into smaller systems of linear equations, see Motsa [1]. The method has been applied to various science and engineering problems described by coupled nonlinear systems of ordinary or partial differential equations. The basic idea of the SRM approach is simple decoupling and rearranging the governing nonlinear equations in a Gauss-Seidel approach to obtain a linear system of equations. The resulting SRM iterative scheme is then integrated using the chebyshev spectral collocation method to obtain the numerical solution. The method was introduced by Motsa and Makukula [2] for the solution of the steady von Karman flow of a Reiner-Rivlin fluid with Joule heating and viscous dissipation. The SRM approach gave accurate results and it was noted that the speed of convergence of the SRM scheme can be significantly improved by using successive over relaxation (SOR) techniques. Shateyi [3] used the SRM to solve the magneto hydrodynamics (MHD) flow and heat transfer in a Maxwell fluid over a stretching surface in a porous medium. The SRM was found to be accurate and rapidly convergent to the numerical results.

Shateyi and Makinde [4] investigated the problem of steady stagnation point flow and heat transfer of an electrically conducting incompressible viscous fluid using the SRM. In Shateyi and Marewo [5], the SRM was applied to magneto-hydrodynamic boundary layer flow with heat and mass transfer in an incompressible upper-convicted Maxwell fluid over a stretching sheet with viscous dissipation and thermal radiation. A generalized presentation of the method was presented in [1] and implemented in three ODEs based systems of boundary layer flow equations of varying complexity. The SRM was found to be an efficient numerical method which gives accurate results, even with only a few grid points. The method has also been successfully applied in obtaining numerical solution of chaotic and hyper-chaotic systems see Motsa et al. [6], Motsa et al. [7], Nik and Rebelo [8], and Dlamini et al. [9]. Motsa et al. [7] extended the SRM to a multistage technique called multistage spectral

relaxation method (MSRM) for solving complex nonlinear initial value problems (IVPs) with chaotic properties. The MSRM was found to be an accurate, efficient, and reliable method for solving very complex IVPs with chaotic behaviour. Nikand Rebelo[8] applied the MSRM in solving hyper-chaotic complex systems and the accuracy and validity of MSRM was tested against Matlab Runge-Kutta based inbuilt solvers and against previously published results.

Motsa et al. [10] extended the application of SRM to systems of nonlinear partial differential equations (PDEs) that model unsteady boundary layer flow. The accuracy of SRM in solving nonlinear PDEs was determined by comparing the computational performance of the SRM against the spectral quasi-linearisation method (SQLM) and Keller-box finite difference scheme The SRM was found to be more efficient in terms of computational accuracy and speed compared to the SQLM and Keller-box method. Awad et al. [11] used the SRM to solve the coupled highly nonlinear system of partial differential equations due to an unsteady flow over a stretching surface in an incompressible rotating viscous fluid in presence of binary chemical reaction and Arrhenius activation energy. Recently, Haroun et al. [12] applied SRM to unsteady MHD mixed convection in a nanofluid due to a stretching/shrinking surface with suction/injection. They reported that SRM is an accurate technique for solving nonlinear boundary value problems. In this course we will use the SRM to solve systems of highly nonlinear ODEs that describe some fluids, flow, heat and mass transfer.

Chapter 2

The spectral method:-

The spectral methods are very powerful tools used to solve ordinary differential equations defined on simple domain and having smooth solutions. They have been widely used due to its high order of accuracy than other alternative numerical methods such as the finite elements, finite differences and finite volume methods. This means that a number of grid points needed to achieve the desired precision is very low, thus spectral methods require less memory than related numerical methods. Spectral methods approximate functions by means of truncated series of orthogonal functions. These functions include the Fourier series for periodic problems, the chebyshev and Legendre polynomials for non-periodic polynomials. More details of spectral methods are found in studies by Canuto et al. [13], Fornberg [14] and Trefethen [15]. The Chebyshev spectral method which approximate functions by the Chebyshev polynomials will be used in this study. We define the k^{th} order Chebyshev polynomials $T_k(x)$ by

$$T_k(x) = cos(k \operatorname{arccos}(x)); k \in \mathbb{N},$$
 (2.1)

in the interval [-1,1].

An unknown, continues function say u(x) can be approximated at $x=x_j$ by a linear combination of Chebyshev polynomials

$$u_N(x_j) = \sum_{k=0}^{N} u_k T_k(x_j), \qquad j = 0, 1, \dots N,$$
 (2.2)

where u_k are the coefficients of the expansion and x_j are the Gauss- Lobatto collocation points defined by

$$x_j = \cos\left(\frac{j\pi}{N}\right),\tag{2.3}$$

with N being the number of collocation points used. Derivatives of the unknown function u(x) at collocation points are obtained as powers of the Chebyshev spectral differentiation matrix \boldsymbol{D} in the form

$$u^{p}(x_{j}) = \sum_{k=0}^{p} \mathbf{D}_{kj}^{p} u(x_{j}), \tag{2.4}$$

where p is the order of differentiation. Entries of the differentiation matrix ${\bf \it D}$ are defined as follows

$$D_{00} = \frac{2N^2 + 1}{6},\tag{2.5}$$

$$D_{jk} = \frac{C_j(-1)^{j+k}}{c_k z_j - z_k} , \qquad j \neq k, \ j = k = 0,1,2 \dots N$$
 (2.6)

$$D_{kk} = \frac{z^k}{2(1-z_k^2)}$$
, $k = 1,2,3...$ (2.8)

where

$$C_k = \left\{ \begin{array}{l} 2 \text{ if } k = 0, \mathbf{N} \\ \\ 1 \text{ if } -1 \leq k \leq \mathbf{N} - 1 \end{array} \right.$$

2.1 Spectral relaxation method (SRM):-

Consider a system of n non-linear ordinary differential equations in n unknowns functions $z_i(\eta)$ (i=1,2,3,...n) where $\eta \in [a,b]$ is the dependent variable. Define the vector Z_i to be the vector of the derivatives of the variable z_i with respect to η , that is

$$Z_i(\eta) = \left[z_i^{(0)}, z_i^{(1)}, \dots z_i^{(q_i)} \right], \tag{2.9}$$

where $z_i^{(0)}=z_i$ and $z_i^{(r)}$ is the r^{th} derivative of z_i with respect to η and $q_i(i=1,2,...,n)$ is thehighest derivative order of the variable z_i appearing in the system of equations. The system can be written in terms of z_i as a sum of its linear (\mathcal{L}) and non-linear components (\mathcal{N}) as

$$\mathcal{L}[Z_1, Z_2, \dots, Z_n] + \mathcal{N}[Z_1, Z_2, \dots, Z_n] = G_i(\eta), \qquad i = 1, 2, 3, \dots n, \tag{2.10}$$

where $G_i(\eta)$ is a known function of η . For illustrative purposes, we assume that equation (2.10) is to be solved subject to two-point boundary conditions which are expressed as

$$\sum_{i=0}^{n} \sum_{p=0}^{q_i-1} \beta_{v,i}^{[p]} z_i^{(p)}(a) = R_{a,v}, \qquad v = 1,2,3,\dots, n_a$$
(2.11)

$$\sum_{i=0}^{n} \sum_{p=0}^{q_i-1} \gamma_{\sigma,i}^{[p]} z_i^{(p)}(b) = R_{b,\sigma}, \quad \sigma = 1,2,3,\dots, n_b$$
 (2.12)

where $\beta_{v,i}^{[p]}\gamma_{\sigma,i}^{[p]}$ are the constant coefficients of $z_i^{(p)}$ in the boundary conditions, and n_a,n_b are the total number of prescribed boundary conditions at η =a and η =b respectively.

Starting from an initial approximation $z_{1,0}, z_{2,0}, z_{3,0}, \dots \dots z_{n,0}$ the iterative technique is obtained as

$$\mathcal{L}_{n-1}[z_{1,r+1}, \dots, z_{n-1,r+1}, z_{n,r}] = G_{n-1} + \mathcal{N}_{n-1}[z_{1,r+1}, \dots, z_{n-2,r+1}, z_{n-1,r}, z_{n,r}],$$

$$\mathcal{L}_{n}[z_{1,r+1}, \dots, z_{n-1,r+1}, z_{n,r+1}] = G_{n} + \mathcal{N}_{n}[z_{1,r+1}, \dots, z_{n-1,r+1}, z_{n,r}],$$
(2.13)

where $z_{i,r+1}$ and $z_{i,r}$ are the approximations of z_i at the current and the previous iteration, respectively. We note that equation (2.13) forms a system of n linear decoupled equations which can be solved iteratively for r=1,2,... starting from a given initial approximation $z_{i,0}$. The iteration is repeated until convergence is achieved. The desired convergence can be assessed by considering the error due to the decoupling of the governing equations. This decoupling error (E_d) at the $(r+1)^{th}$ iteration is defined using the following formula

$$E_{d} = Max \left(\left\| z_{1,r+1} - z_{1,r} \right\|_{\infty}, \left\| z_{2,r+1} - z_{2,r} \right\|_{\infty}, \dots, \left\| z_{n,r+1} - z_{n,r} \right\|_{\infty} \right). \tag{2.14}$$

The idea used in the development of the iteration scheme (2.13) is imported from the Gauss-Seidel relaxation method for solving large systems of algebraic equations. To solve the iteration scheme (2.13), it is convenient to use the Chebyshev pseudo-spectral method. For this reason the method is referred to as the Spectral Gauss-Seidel relaxation method or simply Spectral Relaxation method (SRM) in this work. For brevity, we omit the details of the spectral methods, and refer interested readers to ([16, 24]). Before applying the spectral

method, it is convenient to transform the domain on which the governing equation is defined to the interval [-1,1] on which the spectral method can be implemented. We use the transformation $\eta = \frac{(b-a)(\tau+1)}{2}$ to map the interval [a,b] to [-1,1]. The basic idea behind the spectral collocation method is the introduction of a differentiation matrix ${\bf D}$ which is used to approximate the derivatives of the unknown variables $Z_i(\eta)$ at the collocation points as the matrix vector product

$$\frac{dz_i}{d\eta} = \sum_{k=0}^{N} \mathbf{D}_{jk} z_i(x_k) = DZ_i, \quad j = 1, 2, ..., N$$
(2.15)

where (N + 1) is the number of collocation points (grid points) $\mathbf{D} = 2D/(b-a)$ and $Z = [z(x_0), z(x_1), ..., z(x_N)]^T$ is the vector function at the collocation points. Higher order derivatives are obtained as powers of \mathbf{D} , that is

$$Z_i^{(p)} = \mathbf{D}^p \mathbf{Z}_i. \tag{2.16}$$

In order to apply the Chebyshev differentiation approach to the governing equation (2.9) and iteration scheme (2.13), we observe that equation (2.9) is equivalent to

$$\sum_{i=0}^{n} \sum_{p=0}^{q_i} \alpha_{i,j}^{[p]} z_j^{(p)} + \mathcal{N}_i[z_1, z_2, \dots z_n] = G_i,$$
(2.17)

Where $\alpha_{i,j}^{[p]}$ are the constant coefficients of $z_j^{(p)}$ the derivative of $z_j(j=1,2,\ldots,n)$, that appears in the i^{th} equation for equation $(i=1,2,3,\ldots,n)$. Thus, in terms of the notation used in equation (2.16), the iteration scheme given in equation (2.13) can be expressed compactly

$$\sum_{j=0}^{i} \sum_{p=0}^{q_i} \alpha_{i,j}^{[p]} z_{j,r+1}^{(p)} = G_i - \sum_{j=i+1}^{n} \sum_{p=0}^{q_i} \alpha_{i,j}^{[p]} z_{j,r}^{(p)} - \mathcal{N}_i [z_{1,r+1}, \dots, z_{k-1,r+1}, \dots z_{n,r}],$$
 (2.18)

for $i=1,2,\ldots,n$. Applying the equation (2.16) on (2.18) and the corresponding boundary conditions we obtain the Spectral Gauss-Seidel relaxation method iteration scheme as

$$\sum_{i=0}^{i} \sum_{p=0}^{q_i} \alpha_{i,j}^{[p]} D^p z_{j,r+1}^{(p)} = G_i - \sum_{i=i+1}^{n} \sum_{p=0}^{q_i} \alpha_{i,j}^{[p]} \mathbf{D}^p z_{j,r}^{(p)} - \mathcal{N}_i [z_{1,r+1}, \dots, z_{k-1,r+1}, \dots z_{n,r}],$$
 (2.19)

Subject to

$$\sum_{j=0}^{n} \sum_{p=0}^{q_i-1} \beta_{v,j}^{[p]} \sum_{k=0}^{N} D_{Nk}^{(p)} z_{j,r+1}(x_k) = H_{a,v}, \qquad v = 1,2,3, \dots, n_a$$
 (2.20)

$$\sum_{j=0}^{n} \sum_{p=0}^{q_i-1} \gamma_{\sigma,j}^{[p]} \sum_{k=0}^{N} D_{Nk}^{(p)} z_{j,r+1}(x_k) = H_{b,\sigma}, \qquad \sigma = 1,2,3,\dots, n_b$$
 (2.21)

Chapter3

On the solution of the SRM for a boundary layer flow with a convective surface boundary condition

3. 1 Mathematical Formulation:-

We consider the problem of hydrodynamic and thermal boundary layer flow over a flat plate in a stream of cold fluid at temperature T_{∞} moving over the top surface of the plate with a uniform velocity U_{∞} . The continuity, momentum, energy and concentration equations describing the flow can be written as

$$\frac{\partial u}{\partial x} + \frac{\partial v}{\partial y} = 0, (3.1)$$

$$u\frac{\partial u}{\partial x} + v\frac{\partial v}{\partial y} = v\frac{\partial^2 u}{\partial y^2} + \frac{\sigma B_0^2}{\rho}(u - U_\infty) + g\beta_T(T - T_\infty) + g\beta_C(C - C_\infty), (3.2)$$

$$u\frac{\partial T}{\partial x} + v\frac{\partial T}{\partial y} = \alpha_m \frac{\partial^2 T}{\partial y^2},\tag{3.3}$$

$$u\frac{\partial C}{\partial x} + v\frac{\partial C}{\partial y} = D_m \frac{\partial^2 C}{\partial y^2},\tag{3.4}$$

where u and v are the x (along the plate) and the y (normal to the plate) components of the velocities, respectively, T and C are the fluid temperature and concentration across the boundary layer, v is the kinematic viscosity of the fluid, and α_m is the thermal diffusivity of the fluid, T_∞ is the free stream temperature, C_∞ is the free stream concentration, D_m is the mass diffusivity, β_T is the thermal expansion coefficient, β_C is the solutal expansion coefficient, ρ is the fluid density, g is gravitational acceleration and σ is the fluid electrical conductivity and B_0 is the applied transverse magnetic field. The velocity boundary conditions can be expressed as

$$u(x,0) = v(x,0) = 0,$$

 $u(x,\infty) = U_{\infty}.$ (3.5)

We assume that the bottom surface of the plate is heated by convection from a hot fluid at temperature T_f which provides aheat transfer coefficient h_f . The

boundary conditions at the plate surface and far into the cold fluid may be written as

$$-k\frac{\partial T}{\partial y} = h_f [T_f - T_w], \qquad C = C_w \text{at} \quad y = 0,$$
(3.6)

$$T = T_{\infty}, \qquad C = C_{\infty}. \tag{3.7}$$

where T_w and C_w are temperature and concentration at the plate surface respectively, k is the thermal conductivity coefficient. To satisfy the continuity equation (3.1), we define the stream function ψ in terms of the velocity by

$$u = \frac{\partial \psi}{\partial y}, v = -\frac{\partial \psi}{\partial x},\tag{3.8}$$

and introduce the following dimensionless variables

$$\eta = y \sqrt{\frac{U_{\infty}}{vx}}, \qquad f(\eta) = \frac{\psi}{U_{\infty} \sqrt{\frac{vx}{U_{\infty}}}}, \qquad \theta = \frac{T - T_{\infty}}{T_f - T_{\infty}}, \qquad \phi = \frac{C - C_{\infty}}{C_w - C_{\infty}}.$$
(3.9)

Equations (3.2) - (3.7) reduced to the coupled system of nonlinear differential equations

$$f''' + \frac{1}{2}ff'' - \text{Ha}_{x}(f' - 1) - \text{Gr}_{x}\theta - \text{Gc}_{x}\phi = 0, \tag{3.10}$$

$$\theta'' + \frac{1}{2} \Pr f \theta' = 0, \tag{3.11}$$

$$\phi'' + \frac{1}{2} Sc f \phi' = 0, \tag{3.12}$$

where the prime symbol represent the derivative with respect to η subject to the boundary conditions

$$f(0) = 0, f'(0) = 0, \ \theta'(0) = \text{Bi}_{x}[\theta(0) - 1],$$
 (3.13)

$$\phi(0) = 1, f'(\infty) = 1, \theta(\infty) = \phi(\infty) = 0, \tag{3.14}$$

where $f(\eta)$, $\theta(\eta)$ and $\phi(\eta)$ are the dimensionless velocity temperature and concentration. The parameters of primary interest are the Magnetic field parameter Ha_x , the thermal Grashof number Gr_x , the solutal Grashof number Gc_x , the convective heat transfer parameter Bi_x , the Prandtl number Pr , the Schmidt number Sc given by

$$\mathrm{Ha}_{x}=rac{\sigma B_{0}^{2}x}{
ho U_{\infty}}, \qquad \mathrm{Gr}_{x}=rac{geta_{T}(T_{w}-T_{\infty})x}{U_{\infty}^{2}}, \qquad \mathrm{Gc}_{x}=rac{geta_{C}(C_{w}-C_{\infty})x}{U_{\infty}^{2}},$$

$$\mathrm{Bi}_{x} = rac{h_{f}}{k} \sqrt{rac{vx}{U_{\infty}}}, \qquad \mathrm{Pr} = rac{v}{lpha_{m}}, \qquad \mathrm{Sc} = rac{v}{D_{m}}.$$

3.2 Numerical solution:-

In this section we present the numerical method used to solve the governing nonlinear system of ODEs (3.10)–(3.12). The spectral Relaxation method (SRM) approach is used to decouple the equations leading to a linear system which is subsequently solved using the Chebyshev spectral collocation method. The basic idea behind the SRM scheme from the Gauss-Seidel method for decoupling equations. In this regard, the momentum equation (3.10) is solved only for one unknown function; hence the technical is applied only in involving $f(\eta)$ and its derivatives. All other terms are assumed to be known from previous iterations especially the nonlinear terms which involve $f(\eta)$ and its higher derivatives if exist. In the energy equation (3.11), scheme is applicable only to terms involving $\theta(\eta)$ and its derivatives. The terms involving $\phi(\eta)$ together with the nonlinear terms come from $\theta(\eta)$ and its higher derivatives (if exist) are assumed to be known from the previous iteration while the updated solution for $f(\eta)$ at the current iteration is used. Similarly, in the mass transfer equation (3.12), but terms in $f(\eta)$ and $\theta(\eta)$ are as summed to be now known at the current iteration (denoted by (r+1)). Starting from reducing the order of equation (3.10) by assuming $f'(\eta) = g(\eta)$ together with the chosen initial guesses

$$f(\eta) = e^{-\eta} + \eta - 1, \qquad \theta(\eta) = \frac{\text{Bi}_{\chi}}{(\text{Bi}_{\chi} + 1)} e^{-\eta}, \qquad \phi(\eta) = e^{-\eta}$$
 (3.15)

which are satisfied the boundary conditions (3.13) and (3.14). The subsequent solutions for f_r , θ_r , ϕ_r , $r \geq 1$ are obtained by the following iterative technique

$$f'_{r+1} = g_r, f_{r+1}(0) = 0,$$
 (3.16)

$$g_{r+1}^{"} + \frac{1}{2} f_{r+1} g_{r+1}^{"} - \operatorname{Ha}_{x} (g_{r+1} - 1) - \operatorname{Gr}_{x} \theta_{r} - \operatorname{Gc}_{x} \phi_{r} = 0, \tag{3.17}$$

$$\theta_{r+1}^{"} + \frac{1}{2} \Pr f_{r+1} \theta_{r+1}^{"} = 0, \tag{3.18}$$

$$\phi_{r+1}^{"} + \frac{1}{2} \operatorname{Sc} f_{r+1} \phi_{r+1}^{"} = 0, \tag{3.19}$$

subject to

$$g_{r+1}(0)=0,\; \theta_{r+1}'(0)=\mathrm{Bi}_x[\theta(0)_{r+1}-1]\;\mathrm{or}\;\; \theta_{r+1}(0)=0,\; \phi_{r+1}(0)=0,$$
 (3.20)

$$g_{r+1}(\infty) = 1, \ \theta_{r+1}(\infty) = 0, \ \phi_{r+1}(\infty) = 0.$$
 (3.21)

Applying the chebyshev pseudo-spectral method on (3.16) - (3.19) together with the boundary conditions (3.20) and (3.21), we obtained

$$\mathbf{A}_1 f_{r+1} = R_1 , \qquad f_{r+1}(\tau_0) = 0,$$
 (3.22)

$$\mathbf{A_2}g_{r+1} = R_2, \quad g_{r+1}(\tau_0) = 0 \quad g_{r+1}(\tau_N) = 1,$$
 (3.23)

$$\mathbf{A}_3 \theta_{r+1} = R_3$$
, $\theta_{r+1}(\tau_0) = 0$ $\theta_{r+1}(\tau_N) = 0$, (3.24)

$$\mathbf{A}_4 \phi_{r+1} = R_4, \quad \phi_{r+1}(\tau_0) = 1 \quad \phi_{r+1}(\tau_N) = 0,$$
 (3.25)

where

$$\mathbf{A_1} = \mathbf{D}, \qquad \mathbf{R_1} = g_r, \tag{3.26}$$

$$\mathbf{A_2} = \mathbf{D^2} + \mathbf{diag} \left[\frac{1}{2} f_{r+1} \right] \mathbf{D} - \mathbf{Ha_x} \mathbf{I}, \ \mathbf{R_2} = -(\mathbf{Gr_x} \theta_r + \mathbf{Gc_x} \phi_r + \mathbf{Ha_x}),$$
 (3.27)

$$\mathbf{A_3} = \mathbf{D^2} + \mathbf{diag} \left[\frac{1}{2} \operatorname{Pr} f_{r+1} \right] \mathbf{D}, \qquad \mathbf{R_3} = 0, \tag{3.28}$$

$$\mathbf{A_4} = \mathbf{D^2} + \mathbf{diag} \left[\frac{1}{2} \mathbf{Sc} f_{r+1} \right] \mathbf{D}, \qquad \mathbf{R_4} = 0. \tag{3.29}$$

3.3 Results:-

The system of equations governing the thermo-hydrodynamic boundary layer flow has been solved using the spectral relaxation method. The effects of the governing fluid parameters such as the Magnetic field parameter Ha_x , the thermal Grashof number Gr_x , the solutal Grashof number Gc_x , the convective heat transfer parameter Bi_x , the Prandtl number Pr, the Schmidt number Sc, etc. on the velocity, temperature and concentration profiles has been determined and shown in Fig. 1 - 15. In the absence of the Magnetic field and the buoyancy forces, the problem reduces to that considered by Aziz [25] who solved the governing equations using Runge–Kutta–Fehlberg fourth–fifth (RKF45) method.

Table 1: Computations showing comparison with Aziz [25] and Makinde [26] results for $Ha_x = 0$, $Gr_x = Gc_x = 0$, Pr = 0.72 and Sc = 0.63.

				$\theta(0)$		$-\theta'(0)$			
Bi	It	L	Aziz[25]	Makinde[26]	Present	[25]	[26]	Present	
0.05	21	11	0.1447	0.14466	0.1446612005	0.0428	0.04276	0.0427669400	
0.10	_	_	0.2528	0.25275	0.2527581095	0.0747	0.07472	0.0747241891	
0.20	_	_	0.4035	0.40352	0.4035226075	0.1193	0.11929	0.1192954785	
0.40	_	_	0.5750	0.57501	0.5750140473	0.1700	0.16999	0.1699943811	
0.60	_	_	0.6699	0.66991	0.6699156239	0.1981	0.19805	0.1980506257	
0.80	_	_	0.7302	0.73016	0.7301700557	0.2159	0.21586	0.2158639555	
1.00	_	_	0.7718	0.77182	0.7718222042	0.2282	0.22817	0.2281777958	
5.00	_	_	0.9441	0.94417	0.9441738017	0.2791	0.27913	0.2791309913	
10.0	_	_	0.9713	0.97128	0.9712853870	0.2871	0.28714	0.2871461297	
20.0	_	_	0.9854	0.98543	0.9854335587	0.2913	0.29132	0.2913288270	

The problem would also be in the same line with the study by Makinde [26] who used the Runge–Kutta integration scheme with a modified version of the Newton–Raphson shooting method to solve the governing equations. The results from these previous studies are used as a benchmark to verify the accuracy of our solution.

Table 2: Computations showing comparison with Aziz [25] and Makinde [26] results for $Ha_x=0$, $Gr_x=Gc_x=0$, Pr=0.72 and Sc=0.63.

Bi_{x}	Gr_x	Gc_x	Ha _x	Sc		$-\theta'(0)$	$\theta(0)$			$-\phi(0)$
					[27]	present	[27]	present	[27]	present
0.1	0.1	0.1	0.1	0.24	0.07707	0.0770723	0.22929	0.2292762	0.21859	0.2182949
1.0	0.1	0.1	0.1	0.24	0.25501	0.2550363	0.74498	0.7449636	0.22169	0.2214094
1.0	0.1	0.1	0.1	0.24	0.33335	0.3333849	0.96666	0.9666615	0.22296	0.2226845
0.1	0.5	0.1	0.1	0.24	0.07760	0.0776081	0.22393	0.2239183	0.22381	0.2235437
0.1	1.0	0.1	0.1	0.24	0.07815	0.0781513	0.21849	0.2184864	0.22937	0.2291265
0.1	0.1	0.5	0.1	0.24	0.07969	0.0796957	0.20306	0.2030420	0.24852	0.2484029
0.1	0.1	1.0	0.1	0.24	0.08143	0.0814392	0.18562	0.1856079	0.27339	0.2733431
0.1	0.1	0.1	0.5	0.24	0.07875	0.0787560	0.21244	0.2124392	0.23452	0.2342787
0.1	0.1	0.1	1.0	0.24	0.08034	0.0780936	0.19652	0.2190636	0.25077	0.2278222
0.1	0.1	0.1	0.1	0.62	0.07677	0.0767781	0.23221	0.2322182	0.31232	0.3123209
0.1	0.1	0.1	0.1	0.78	0.07671	0.0767128	0.23287	0.2328712	0.33955	0.3395512
0.1	0.1	0.1	0.1	2.62	0.07641	0.0764175	0.23582	0.2358246	0.52053	0.5205280

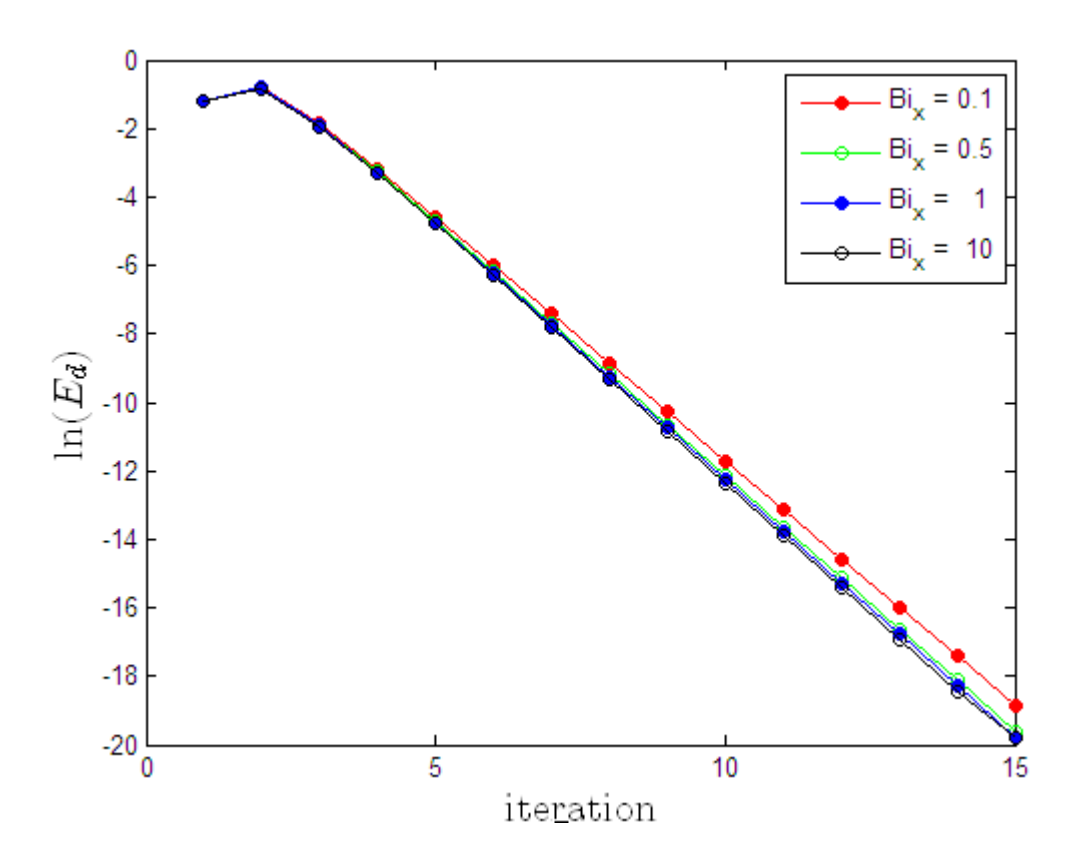


Fig. 1: Effect of parameter ${\rm Bi}_x$ on the Logarithm of the SRM error.

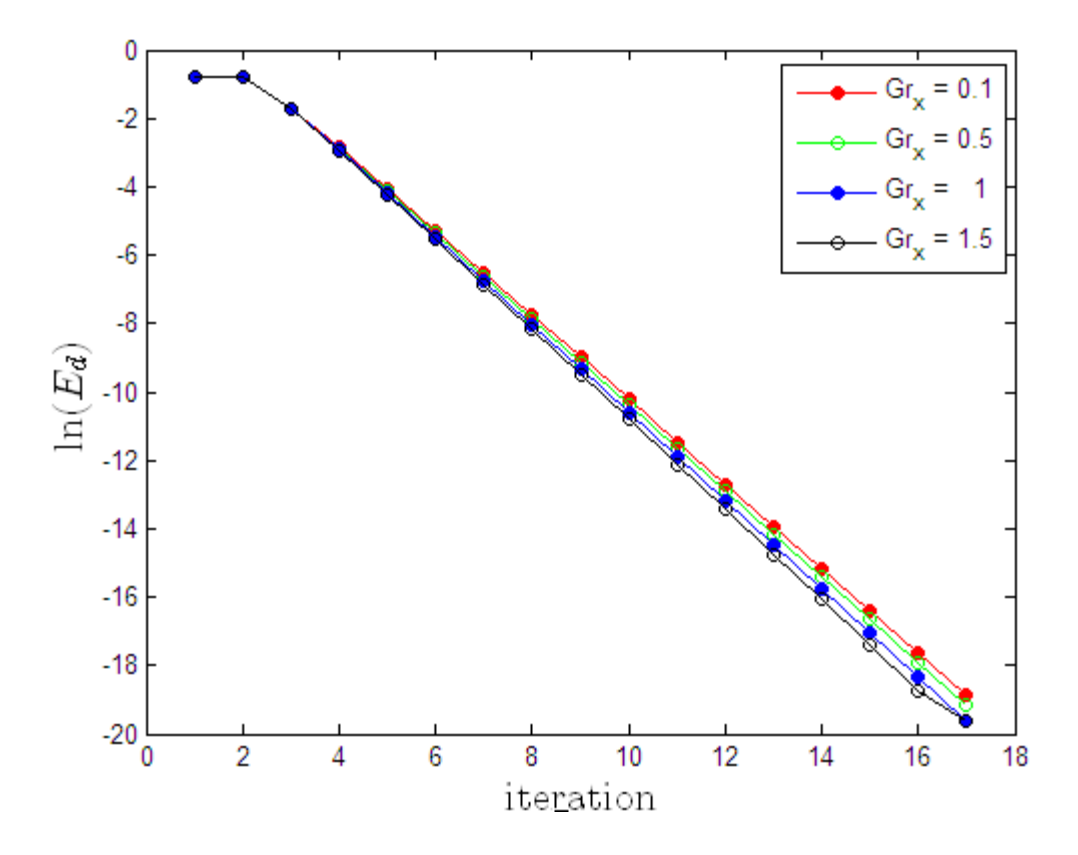


Fig. 2: Effect of parameter Gr_{x} on the Logarithm of the SRM error.

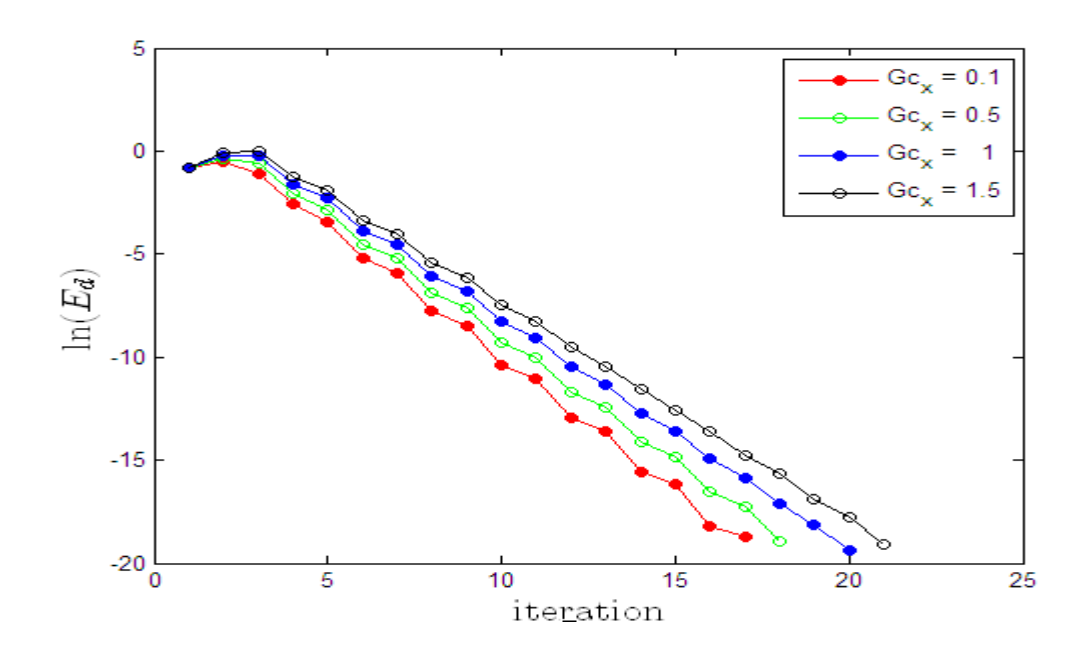


Fig. 3: Effect of parameter Gc_x on the Logarithm of the SRM error.

Fig.1-3 show the variation of the residual error against the number of iterations. As the number of iterations increases, the norm of the residual error of the SRM can be seen to decrease until a point where convergence of the norm is attained. At that point, optimal residual error is said to have been obtained.

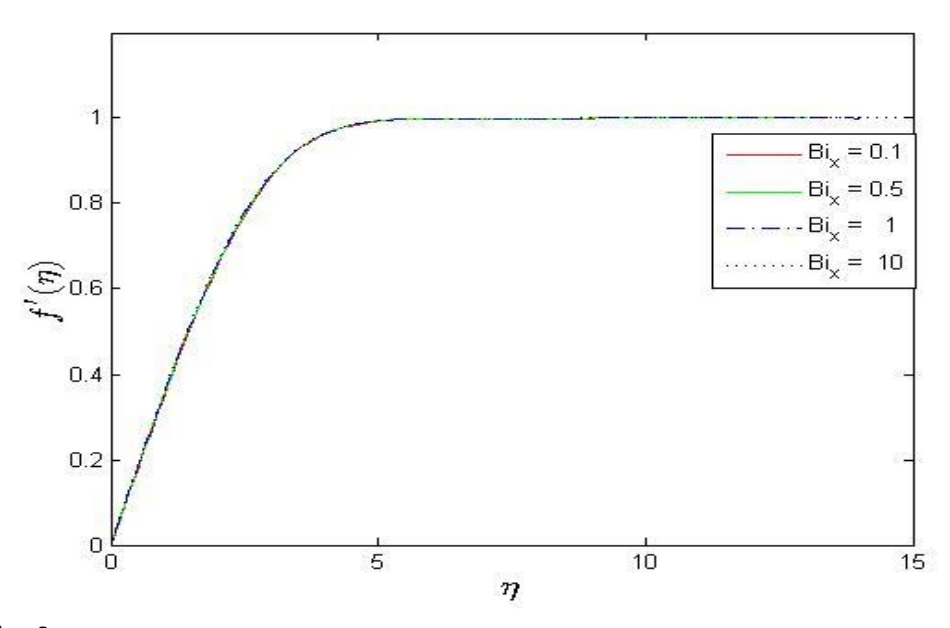


Fig.4: Effect of the convective heat transfer parameter Bi_x on the velocity profile for $Gr_x = Gc_x = 0.1$, $Ha_x = 0.1$, Pr = 0.72 and Sc = 0.24.

The comparison of the plate surface temperature and heat transfer coefficients obtained by the SRM with those reported by Aziz [25] and Makinde [26] is shown in Table 1 and Table 2. It is clear that the SRM results in a good agreement in order of accuracy and convergence.

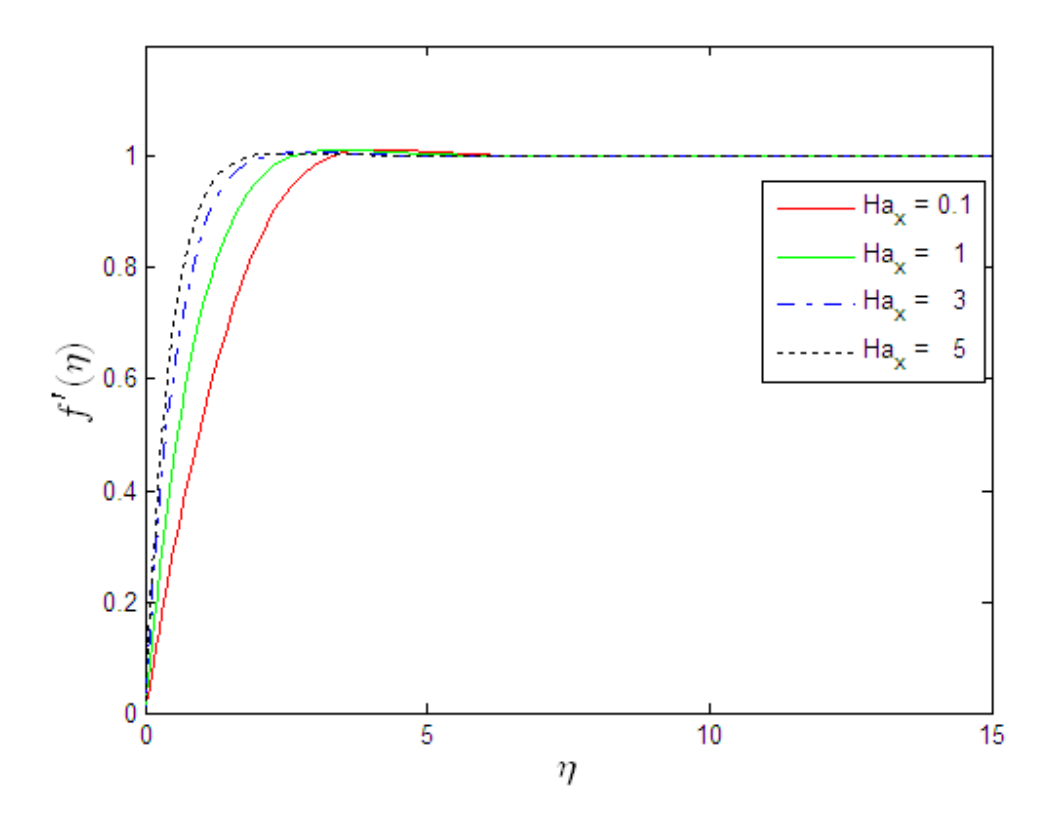


Fig.5: Effect of the magnetic field parameter Ha_x on the velocity profile for $\mathrm{Bi}_x=0.1$, $\mathrm{Gr}_x=\mathrm{Gc}_x=0.1$, $\mathrm{Pr}=0.72$ and $\mathrm{Sc}=0.24$.

Fig. 4 shows the effect of heat convective parameter Bi_x on the velocity profile when the other parameters are held constant. It is clear that the momentum boundary layer thickness decreases with Bi_x that is why the velocity profile increases as the heat transfer parameter increases.

Fig.5 depicts the effect of increasing the magnetic field strength on the momentum boundary-layer thickness. It is now a well-established fact that the magnetic field presents a damping effect on the velocity field by creating a drag force that opposes the fluid motion, causing the velocity to decrease. However, in this case an increase in the Ha_{x} only slightly slows down the motion of the fluid away from the vertical plate surface toward the free stream velocity, while the fluid velocity near the vertical plate surface increases. Similar trend of slight increase in the fluid velocity near the vertical plate is observed with an increase in convective heat transfer parameter.

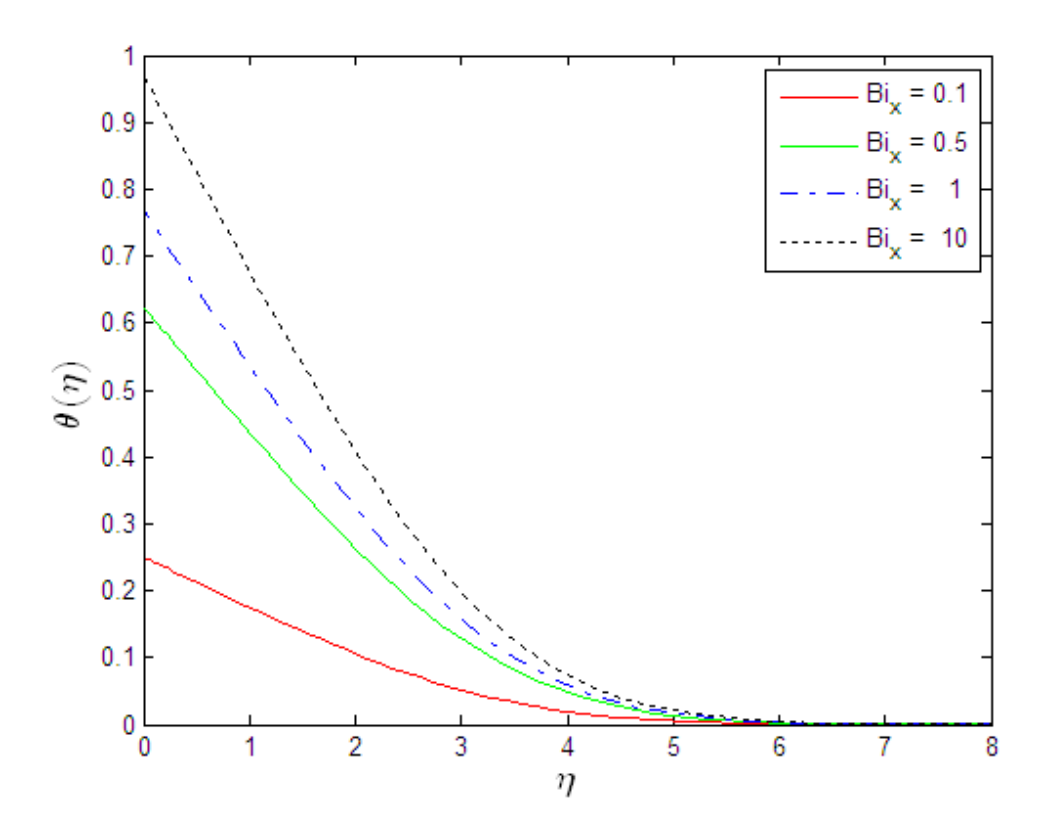


Fig.6: Effect of the convective heat transfer parameter Bi_x on the temperature profile for $Ha_x=0.1$, $Gr_x=Gc_x=0.1$, Pr=0.72 and Sc=0.24.

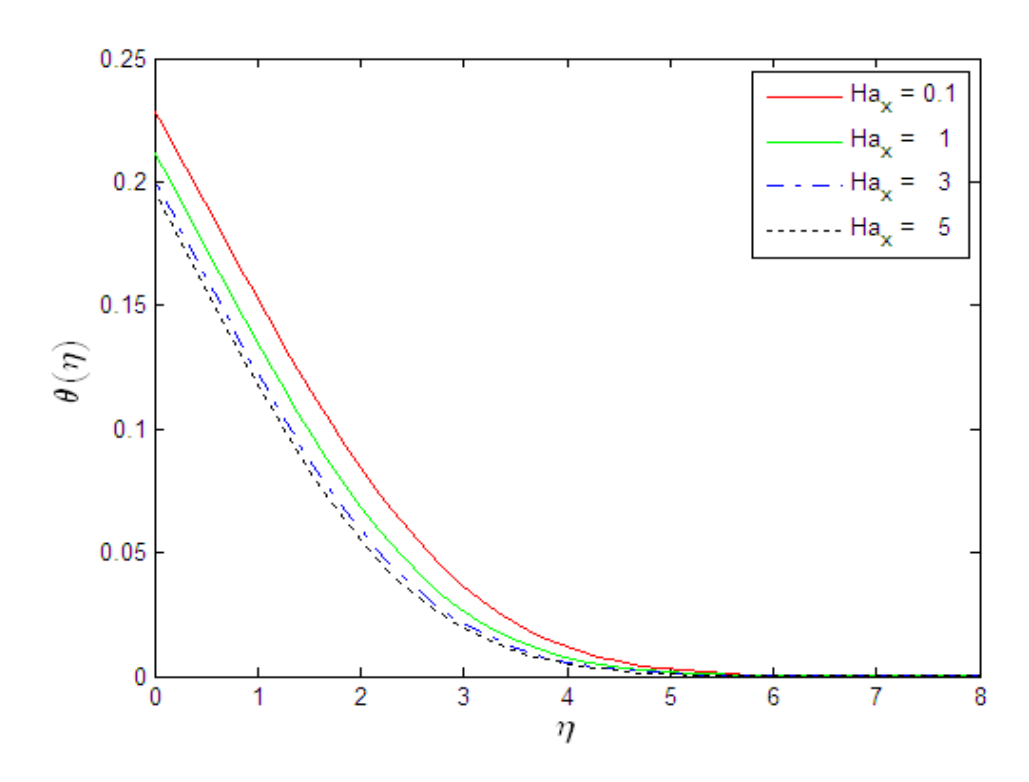


Fig.7: Effect of the magnetic field parameter Ha_x on the temperature profile for $\mathrm{Bi}_x=0.1$, $\mathrm{Gr}_x=\mathrm{Gc}_x=0.1$, $\mathrm{Pr}=0.72$ and $\mathrm{Sc}=0.24$.

Fig.6 demonstrates the effect of ${\rm Bi}_{x}$ on temperature profile. It is evident that the heat convective parameter contributes to increasing the thickness of the thermal boundary layer; consequently, enhance the temperature in the boundary layer.

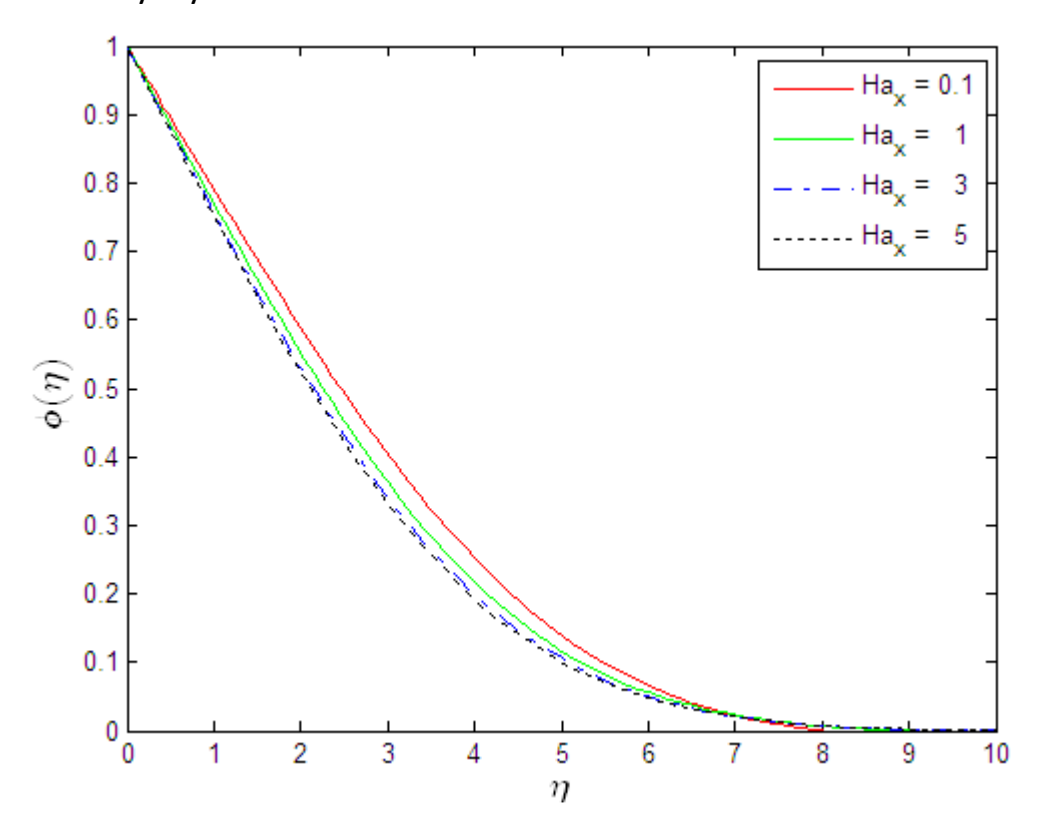


Fig.8: Effect of the magnetic field parameter Ha_x on the concentration profile for $\mathrm{Bi}_x=0.1$, , $\mathrm{Gr}_x=\mathrm{Gc}_x=0.1$, $\mathrm{Pr}=0.72$ and $\mathrm{Sc}=0.24$.

Fig.7 and Fig.8 illustrate the effect of magnetic field Ha_x on both the temperature and concentration profiles respectively. It can be seen easily that the thermal boundary layer thickness increases when the magnetic field increases, thus decreasing the reduced temperature in the boundary layer. On the other hand, as Ha_x increasing the fluid velocity decreases as results of increasing the damping force on the velocity, hence decreasing the mass.

Fig.9 shows the effect of heat convective parameter on the concentration profile. It is clear that increasing Bi_{x} has no significant effect on the mass and its effect can be neglected.

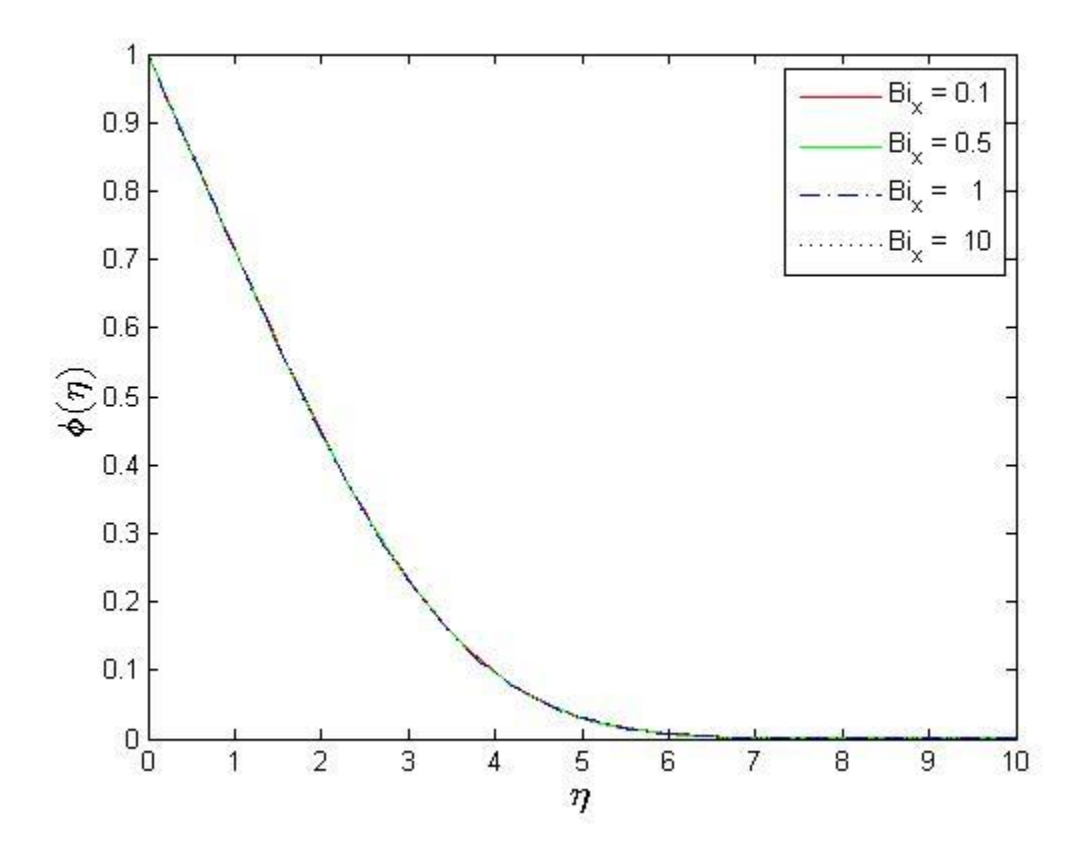


Fig.9: Effect of the convective heat transfer parameter Bi_x on the concentration profile for $Ha_x=0.1$, $Gr_x=Gc_x=0.1$, Pr=0.72 and Sc=0.24.

Fig. 10 – 12 have been plotted in order to see the effect of Gr_x on the velocity, temperature and concentration profiles. It is clear that the velocity increases by increasing Gr_x . Effects Gr_x on the temperature and concentrations are totally opposite, we noted that both the temperature and concentration are increasing functions on Grashof.

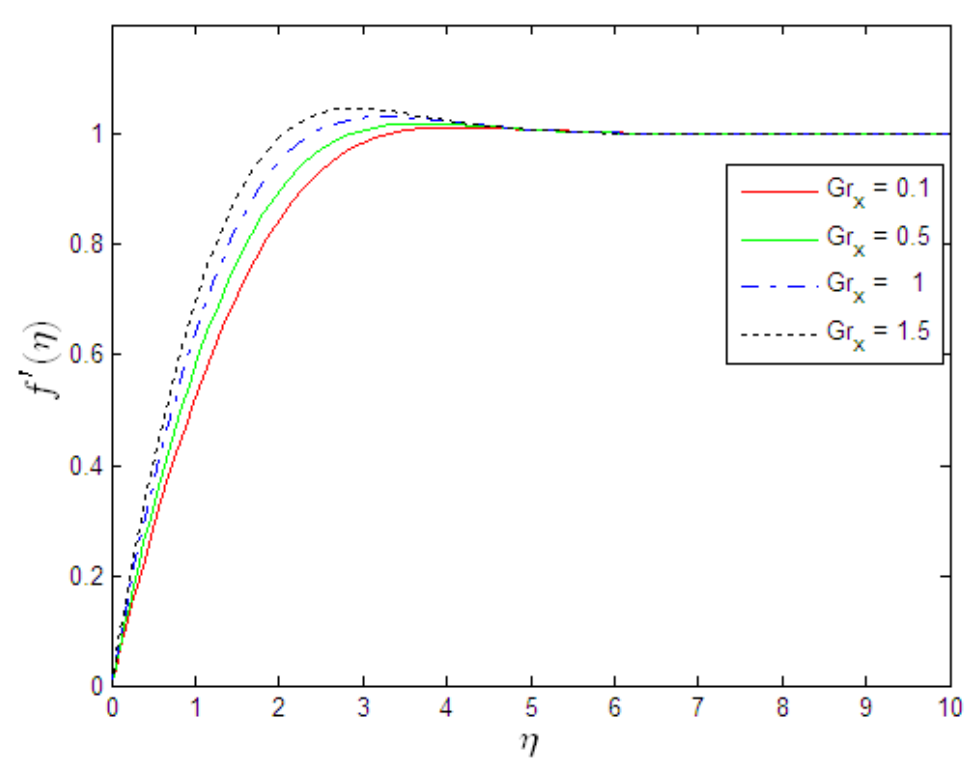


Fig.10: Effect of the Grashof number Gr_x on the velocity profile for $Ha_x=0.1$, $Bi_x=0.1$, $Gc_x=0.1$, Pr=0.72 and Sc=0.24.

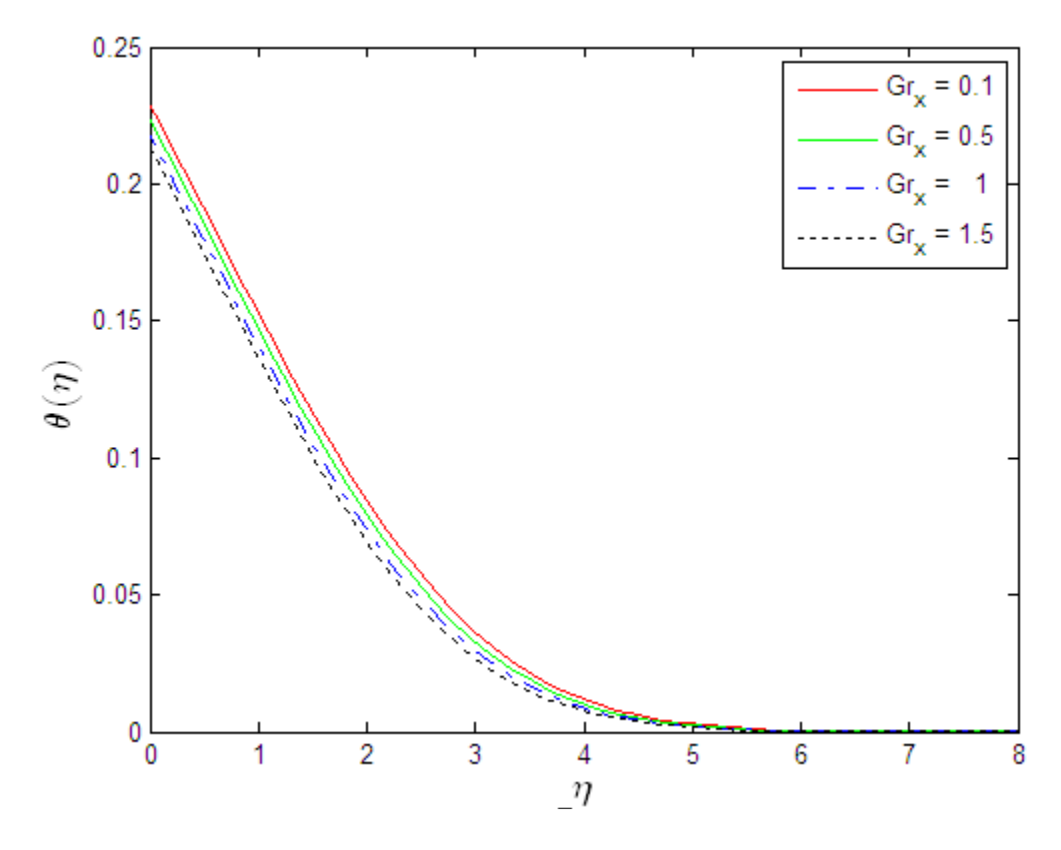


Fig.11: Effect of the Grashof number Gr_x on the temperature profile for $Ha_x=0.1$, $Bi_x=0.1$, $Gc_x=0.1$, Pr=0.72 and Sc=0.24.

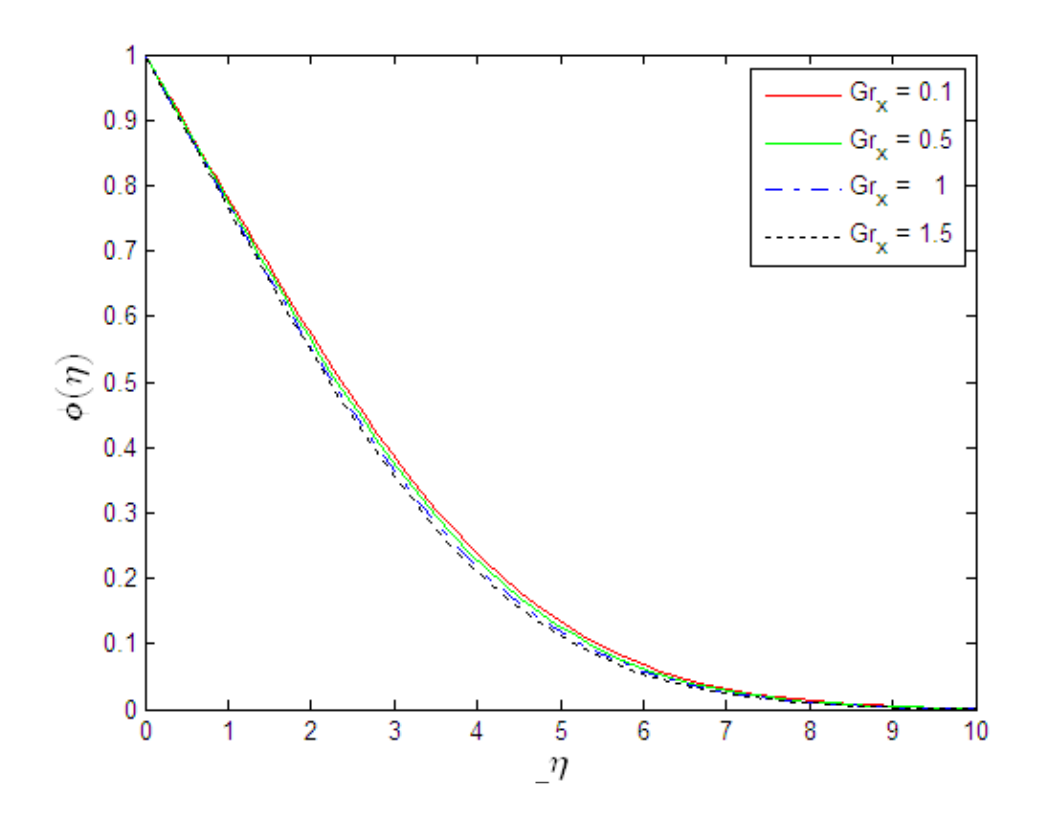


Fig.12: Effect of the Grashof number Gr_x on the concentration profile for $Ha_x = 0.1$, $Bi_x = 0.1$, $Gc_x = 0.1$, Pr = 0.72 and Sc = 0.24.

Fig.13 shows the effects of solutal Grashof number Gc_{χ} on the velocity field $f'(\eta)$. It can be seen that the momentum boundary layer thinness increases when the solutal Grashof number Gc_{χ} increases, thus increasing the velocity $f'(\eta)$.

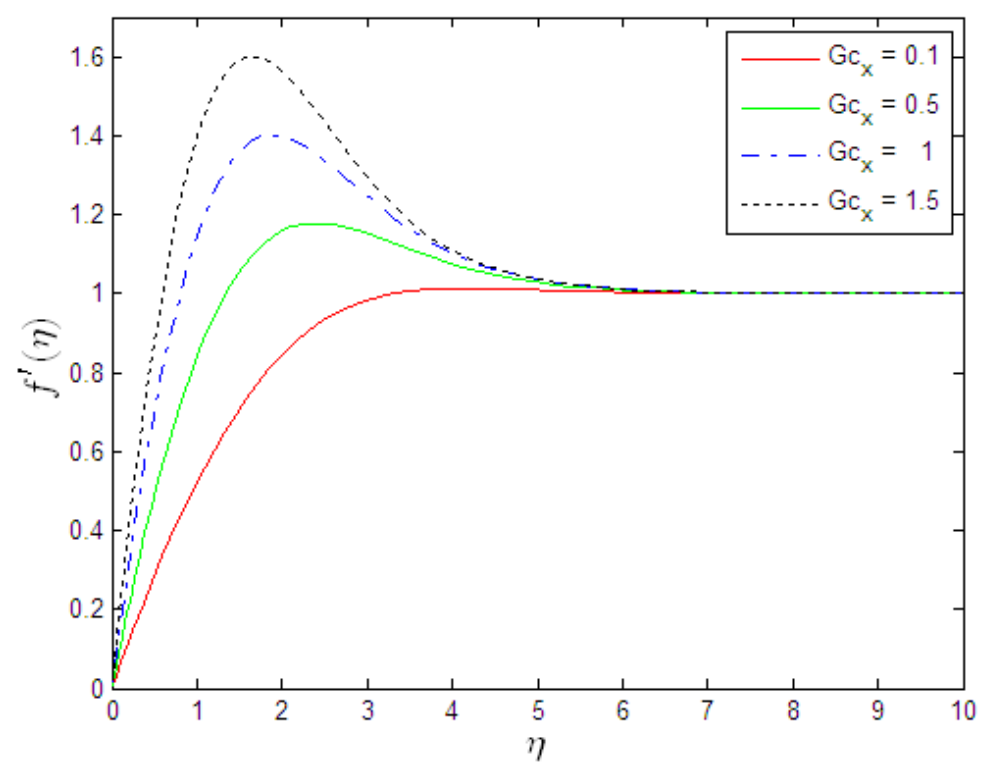


Fig.13: Effect of the solutal Grashof number Gc_x velocity profile for $Bi_x = 0.1$, $Ha_x = 0.1$, $Gc_x = 0.1$, Pr = 0.72 and Sc = 0.24.

Fig. 14 and 15 show the variation of the temperature and concentration profiles for difference values of the solutal Groshof number Gc_x . It is clear that when Gc_x increases, both the temperature and concentration distributions decrease thus diminishing the thicknesses of both the thermal and concentration boundary layers.

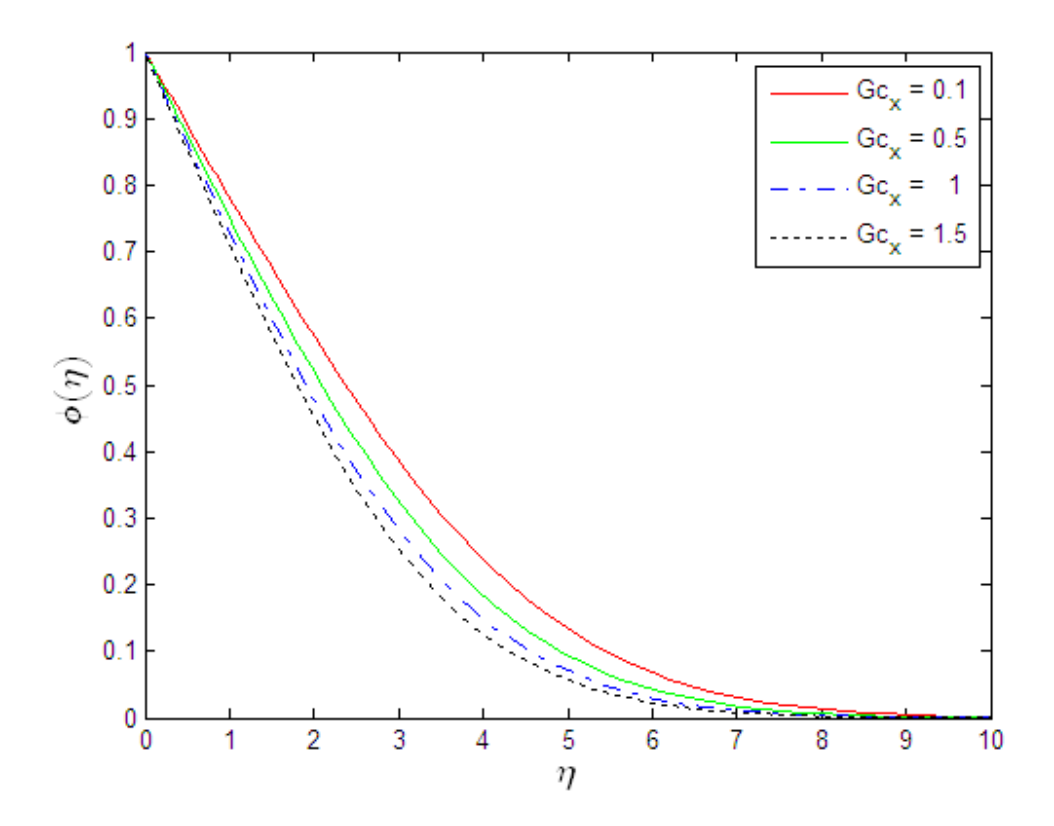


Fig.14: Effect of the solutal Grashof number Gc_x concentration profile for $Ha_x = 0.1$, $Bi_x = 0.1$, $Gr_x = 0.1$, Pr = 0.72 and Sc = 0.24.

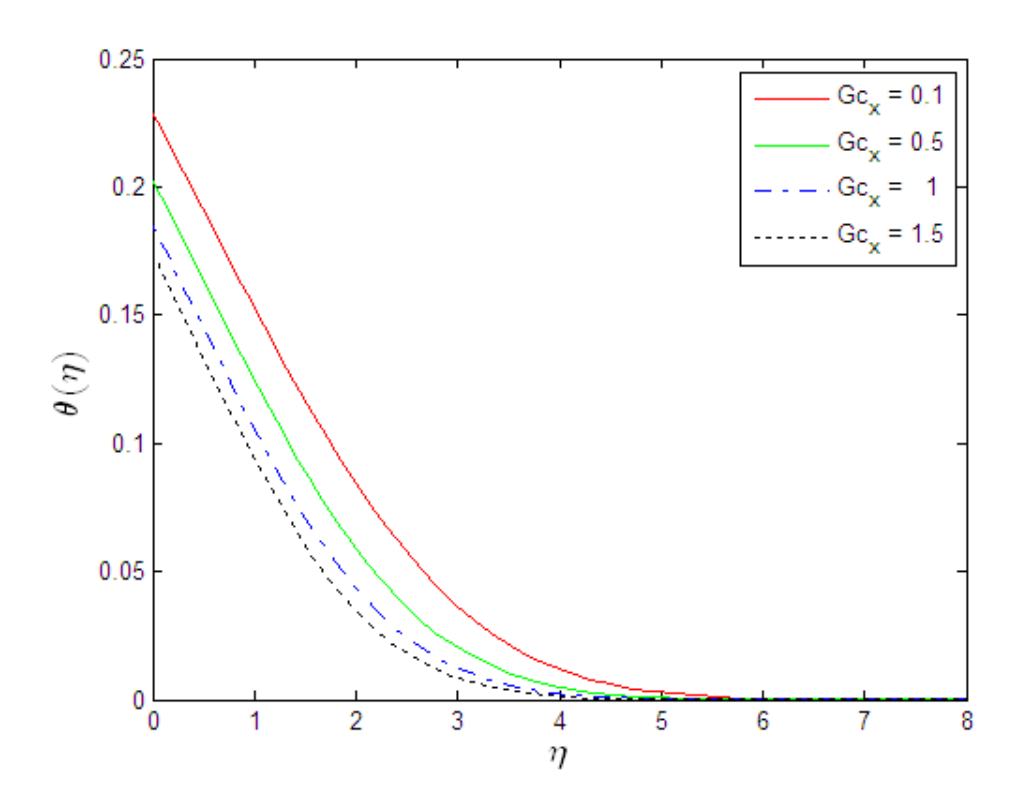


Fig. 15: Effect of the solutal Grashof number Gc_x temperature profile $Bi_x=0.1$, $Ha_x=0.1$, $Gr_x=0.1$, Pr=0.72 and Sc=0.24.

Chapter 4

Dufour and Soret effects on incompressible Newtonian fluid flow over a vertical down-pointing cone

4-1.Mathematical Function:-

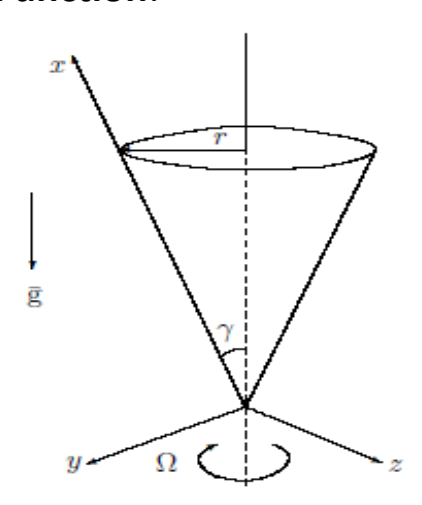


Fig. 1: Schematic sketch of a spinning vertical cone

Consider resulting ordinary differential equations obtained by Narayna et al. [28] which governing an incompressible Newtonian fluid flow over a vertical downpointing cone. The x-axis assume to be along the surface of the cone and y-axis along the outward normal surface of the cone with origin being the vortex of the cone (see Fig. 1). Assume that the cone rotate about its axis of symmetry with angular velocity g, moreover an external magnetic field is applied along the y-axis. The surface of the cone is subject to either a linear surface temperature (LST) or the linear surface heat flux (LSHF) for more details see Narayana et al. [28]. The momentum, energy and concentration governing equations can be presented in the following form.

$$f''' + 2ff'' - f'^{2} + \epsilon g^{2} + \theta + N\phi - Mf' = 0, \tag{4.1}$$

$$g'' + 2fg' - 2f'g - Mg = 0, (4.2)$$

$$\theta'' + \Pr(2f\theta' - f'\theta) + \mathcal{D}_f \phi'' = 0, \qquad (4.3)$$

$$\phi'' + \text{Sc}(2f\phi' - f'\phi) + \text{Sr}\theta'' = 0, \tag{4.4}$$

subject to the boundary conditions

$$f(0) = f'(0) = 0, \ g(0) = 1, \ \theta(0) = 1, \text{ or } \theta'(0) = -1, \ \phi(0) = 1$$
$$f'(\infty) \to 0, g(\infty) \to 0, \theta(\infty) \to 0, \phi(\infty) \to 0. \tag{4.5}$$

4-2. Numaracal solution:-

To apply the SRM on the system (4.1) – (4.4) along with the boundary conditions (4.5), we have to reduce the order of equation (4.1) by assuming $f'(\eta) = h(\eta)$, so the iteration scheme can be written in following form

$$f'_{r+1} = h_r$$
, $f_{r+1}(0) = 0$, (4.6)

$$h_{r+1}^{"} + 2f_{r+1}h_{r+1}^{"} - Mh_{r+1} = h_r^2 - \epsilon g_r^2 + \theta_r + N\phi_r, \tag{4.7}$$

$$g_{r+1}^{"} + 2f_{r+1}g_{r+1}^{"} - 2h_{r+1}g_{r+1} - Mg_{r+1} = 0, (4.8)$$

$$\theta_{r+1}^{"} + 2\Pr f_{r+1}\theta_{r+1}^{"} - \Pr h_{r+1}\theta_{r+1} = -D_f \phi_r, \tag{4.9}$$

$$\phi_{r+1}^{"} + 2\operatorname{Sc} f_{r+1} \phi_{r+1}^{"} - \operatorname{Sc} h_{r+1} \phi_{r+1} = -\operatorname{Sr} \theta_{r+1}^{"}, \tag{4.10}$$

subject to the boundary conditions

$$h_{r+1}(0) = 0$$
, $h_{r+1}(\infty) = 0$, $g_{r+1}(0) = 1$, $g_{r+1}(\infty) = 0$, $\theta_{r+1}(0) = 1$
or $\theta'_{r+1}(0) = -1$, $\theta_{r+1}(\infty) = 0$, $\phi_{r+1}(0) = 1$, $\phi_{r+1}(\infty) = 0$. (4.11)

Applying the chebyshev pseudo-spectral method on (4.1 - 4.4) we obtain

$$\mathbf{A}_1 f_{r+1} = R_1 , \qquad f_{r+1}(\tau_0) = 0$$
 (4.12)

$$\mathbf{A}_2 h_{r+1} = R_2, \qquad h_{r+1}(\tau_0) = 0, \quad h_{r+1}(\tau_N) = 0,$$
 (4.13)

$$\mathbf{A}_3 g_{r+1} = R_3, \qquad g_{r+1}(\tau_0) = 1, \ g_{r+1}(\tau_N) = 0,$$
 (4.14)

$$\mathbf{A}_4 \theta_{r+1} = R_4, \quad \theta_{r+1}(\tau_0) = 1, \quad \theta_{r+1}(\tau_N) = 0,$$
 (4.15)

$$\mathbf{A}_5 \phi_{r+1} = R_5, \quad \phi_{r+1}(\tau_0) = 1, \quad \phi_{r+1}(\tau_N) = 0,$$
 (4.16)

where

$$A_1 = D$$
, $R_1 = h_r$, (4.17)

$$\mathbf{A_2} = \mathbf{D^2} + 2\mathbf{diag}[f_{r+1}]\mathbf{D} - \mathbf{MI}, \ R_2 = h_r^2 - \epsilon g_r^2 - \theta_r - \mathbf{N}\phi_r,$$
 (4.18)

$$\mathbf{A_3} = \mathbf{D^2} + 2\operatorname{diag}[f_{r+1}]\mathbf{D} - 2\operatorname{diag}[h_{r+1}] - \mathbf{MI}, \quad R_3 = 0,$$
 (4.19)

$$\mathbf{A_4} = \mathbf{D^2} + 2\mathbf{diag}[\Pr f_{r+1}]\mathbf{D} - \mathbf{diag}[\Pr h_{r+1}], \qquad R_4 = -D_f \phi_{r+1}'', \qquad (4.20)$$

$$\mathbf{A_5} = \mathbf{D^2} + 2\mathbf{diag}[Scf_{r+1}]\mathbf{D} - \mathbf{diag}[Sch_{r+1}], \qquad R_5 = -S\theta''_{r+1}.$$
 (4.21)

4-3.Results:-

As the exact solution is not feasible for equations (4.1) - (4.4) because of their high nonlinearly, we solved them numerically by using the spectral relaxation method. The proposed SRM method is strongly depends on the length of the governing domain (b - a) and the number N of collocation points (grid points). In particular, since the problem considered in this chapter is defined on the semi-infinite interval $[0,\infty)$, a crucial factor of the SRM iteration scheme is to find the appropriate finite value (η_{∞}) which must be selected to be large enough to numerically approximate infinity and the behaviour of the governing flow parameters at infinity. In order to select the appropriate value of η_{∞} , we start with an initial guess which is relatively small and solve the governing SRM scheme equations over $[0, \eta_{\infty}]$ to obtain the solutions of flow parameters $f(\eta)$, $g(\eta)$, $\theta(\eta)$, $\phi(\eta)$, etc., the values of the derivatives of these functions at $\eta = 0$, such as f''(0), g'(0), $\theta'(0)$, $\phi'(0)$ etc., are also obtained. The current value of η_{∞} is increased by one and the solution process is repeateduntil the difference in the values of f''(0), $\theta(0)$, $\theta'(0)$, etc., between the current and previous solution is less than a specified accuracy tolerance level. Once the optimal value of η_{∞} has been identified for a set of governing physical constants, the minimum value of the number of grid points required to give solutions that do not depend on the grid size is obtained using a similar process. Starting from a small value of N, say N = 30, the SRM scheme is solved for the governing flow parameters. The value of N is increased by 10 and the solution is solved until the results do not change, to with in a certain accuracy tolerance level, with any further increase in N. In order to check the accuracy and validity of the proposed method, the results presented in this study were compared with those of previously published literature for selected values of the governing physical parameters.

In order to verify the accuracy of our solution, the comparison of skin friction coefficient obtained by the SRM with those reported by Ece[27] and Narayana [28] is shown in Table1. It is clear that the SRM results are in a good agreement in order of accuracy.

Analysis has been carried out for different Dufour and Soret parameter values and for several values of the Hartmann number M, the Prandtl number Pr, the Schmidt number Scand the spin parameter ϵ . The results for the skin friction, heat and mass transfer coefficients and the tangential velocity are summarized in Tables 1 - 4. Table 1 give a comparison between the current results and those of Ece [27] and Narayana[28] for a spinning cone in the absence of Dufour and Soret effects. The comparison is given for case of LST. From this table one observes an excellent agreement between the present results and those of Ece[27] and Narayana[28].Fig. 1- 10 show the effects of the various fluid parameters on the axial velocity, temperature and concentration profiles.

Fig. 2(a) - 2(d) show that the effects of the Dufour and Soret parameter with spin parameters on the axial velocity profile are similar in both the LST and LSHF cases the velocity increases as the rate of spin increases.

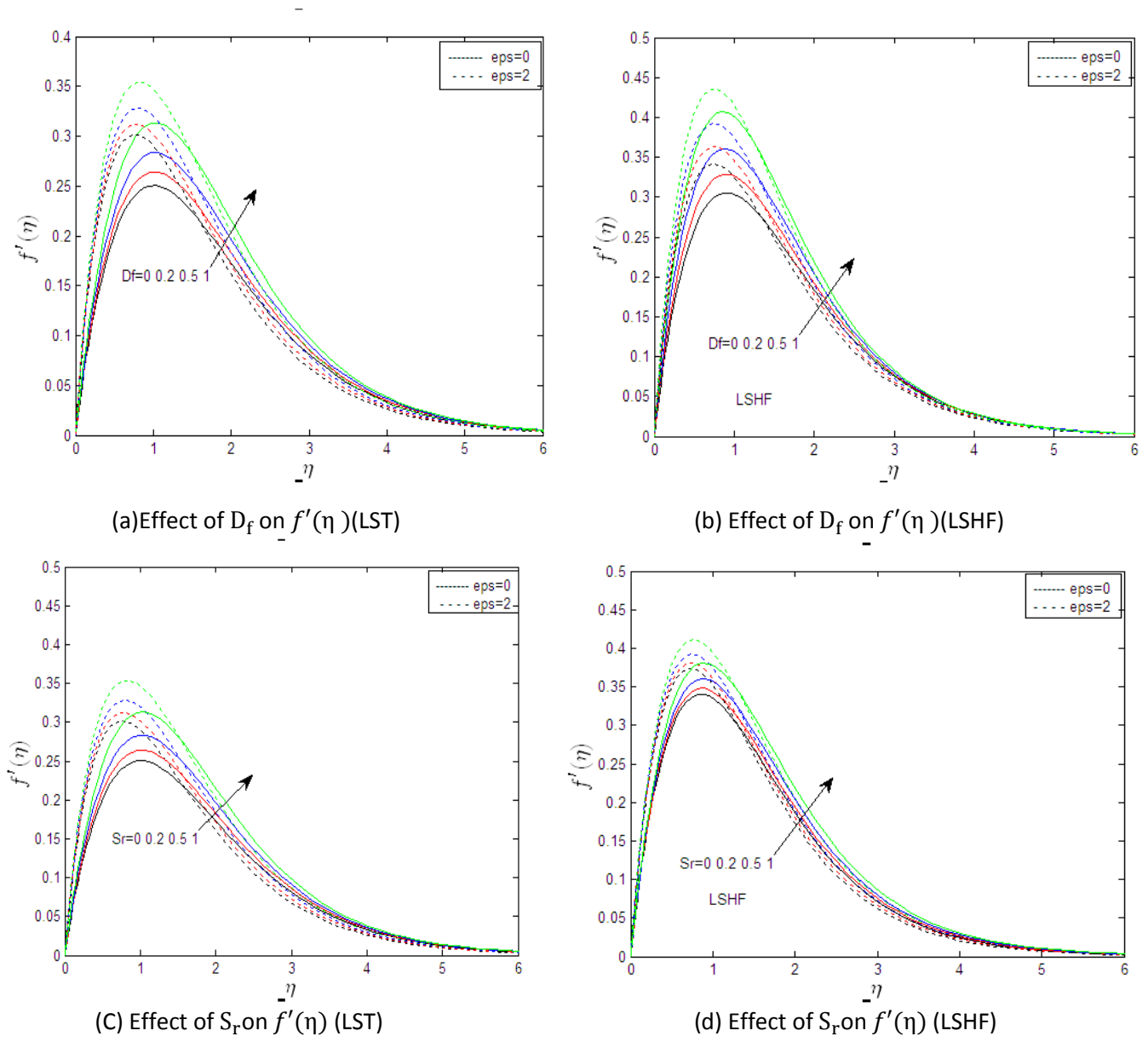


Fig. 2: Variation of axial velocity profiles with Dufour and Soret numbers for different values of spin parameter ϵ .

The axial velocity $f'(\eta)$ is plotted in Fig. 2(a) and (b) for different values of the Dufour and spin parameters in both the LST and LSHF cases. It can be observed that with an increase in the both Dufour and spin parameters the velocity profile increase in the boundary layer.

Fig. 2(c) and (d) show the effect of the Soret parameter on $f'(\eta)$ for different values of the spin parameter. The velocity increases with increasing the Soret parameter. Increasing the diffusion-thermo and thermal-diffusion effects and the spin parameter leads to an increase in the velocity.

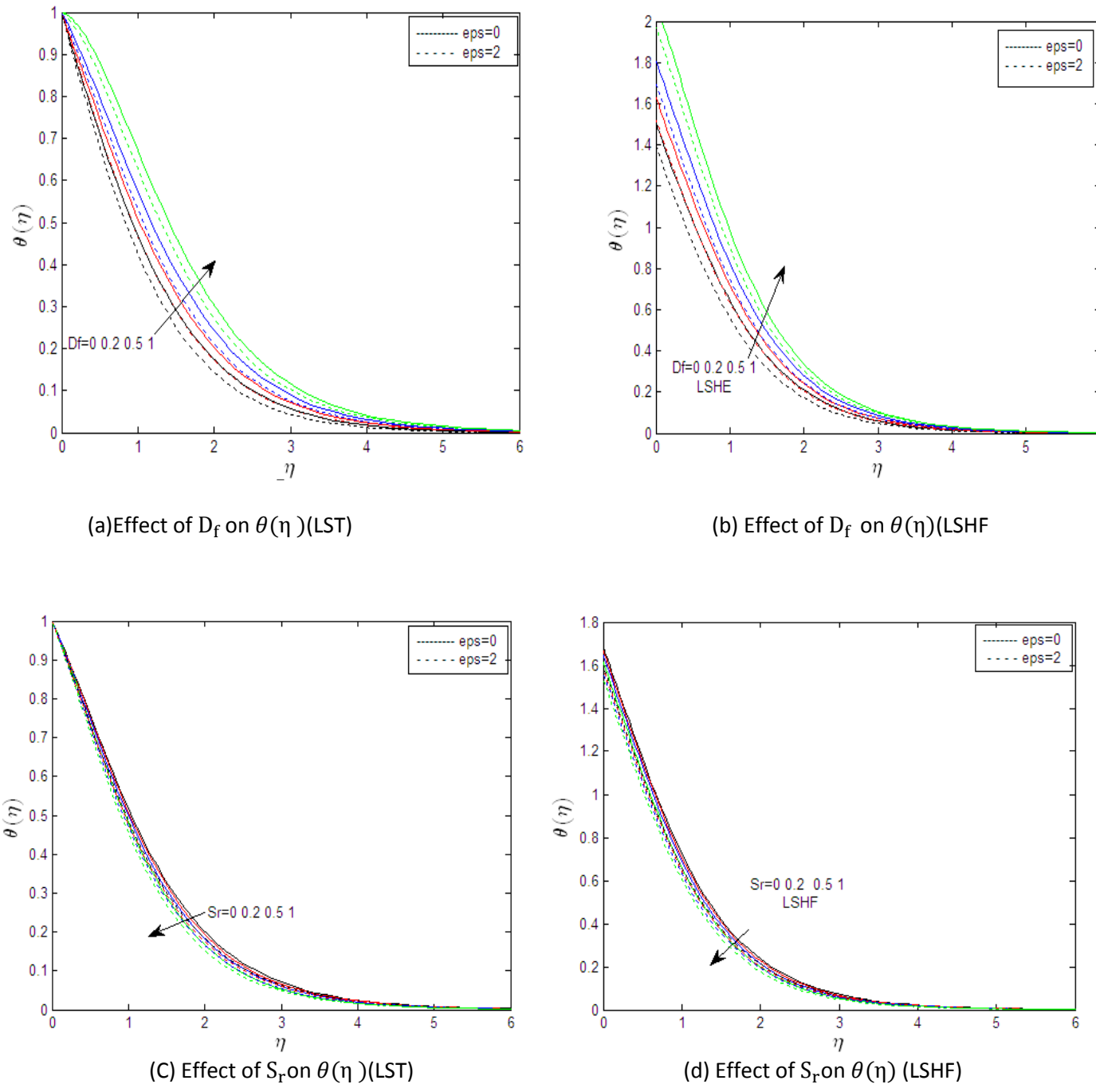


Fig. 3: Variation of temperature profiles with Dufour and Soret numbers for different values of spin parameter ϵ .

Fig. 3 show Dufour and Soert on the temperature for different spin parameter values. We observe firstly that the temperature decreases as the rate of spin increases. Secondly, the temperature increases with the Dufour parameter. However, an increase in the Soret parameter causes a thinning of the thermal

boundary layer causing a drop in the temperature. The temperature profiles are broader for large spin values than in the case of no spin.

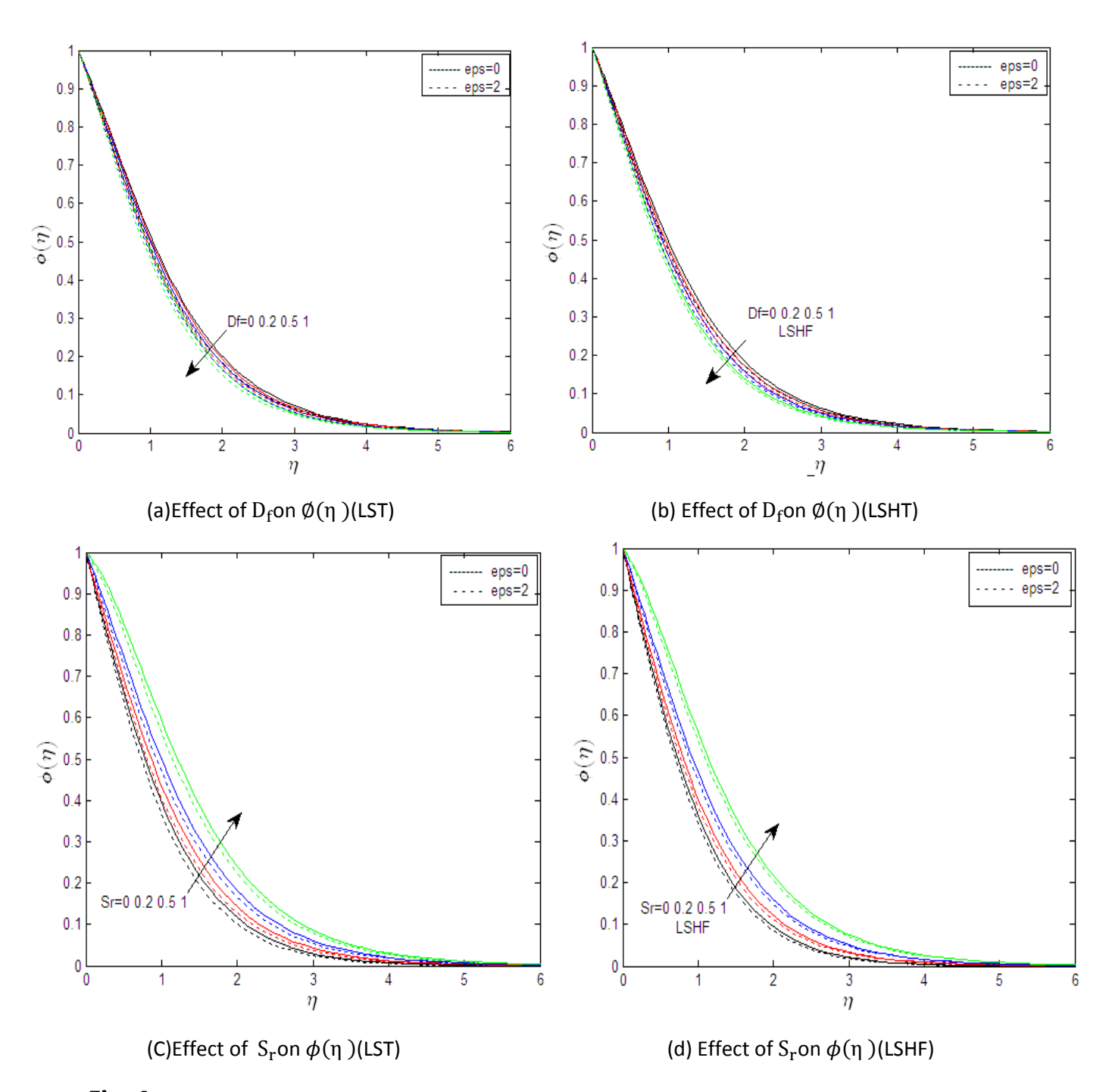


Fig. 4: Variation of axial velocity profiles with Dufour and Soret numbers for different values of spin parameter ϵ .

Fig.4 (a)—(d) show the variation of the concentration profile with Dufour and Soret parameters in both the LST and LSHF cases for a stationary and a spinning cone. Spinning the cone and reducing the Dufour number both lead to a

reduction in the solute concentration whereas increasing the Soret parameter enhances the concentration boundary layer profile in both the LST and LSHF cases. The effect of the magnetic parameter M on the velocity is shown in Fig. 5 in the presence of Dufour and Soret effects. The tangential velocity of the fluid decreases with the Hartmann number due to the presence of a resistive Lorentz force which acts against the flow if the magnetic field is applied in the normal direction. The effect of the magnetic parameter M on temperature and concentration profiles is shown in Fig. 6 and 7 respectively. The slowing down in the motion of the electrically conducting fluid leads to a build-up of heat and solute concentration, and consequently, both temperature and solute concentration increase with increasing Hartmann numbers in the boundary layer region (see Al-Odat and Al-Azab [29]). Fig. 8 shows the effect of the Prandtl number on the axial velocity profile (and Pr=0.7 for air is used in the present study). The Prandtl number has a significant effect on the axial velocity and it is clear that the boundary layer thickness reduces with Pr.

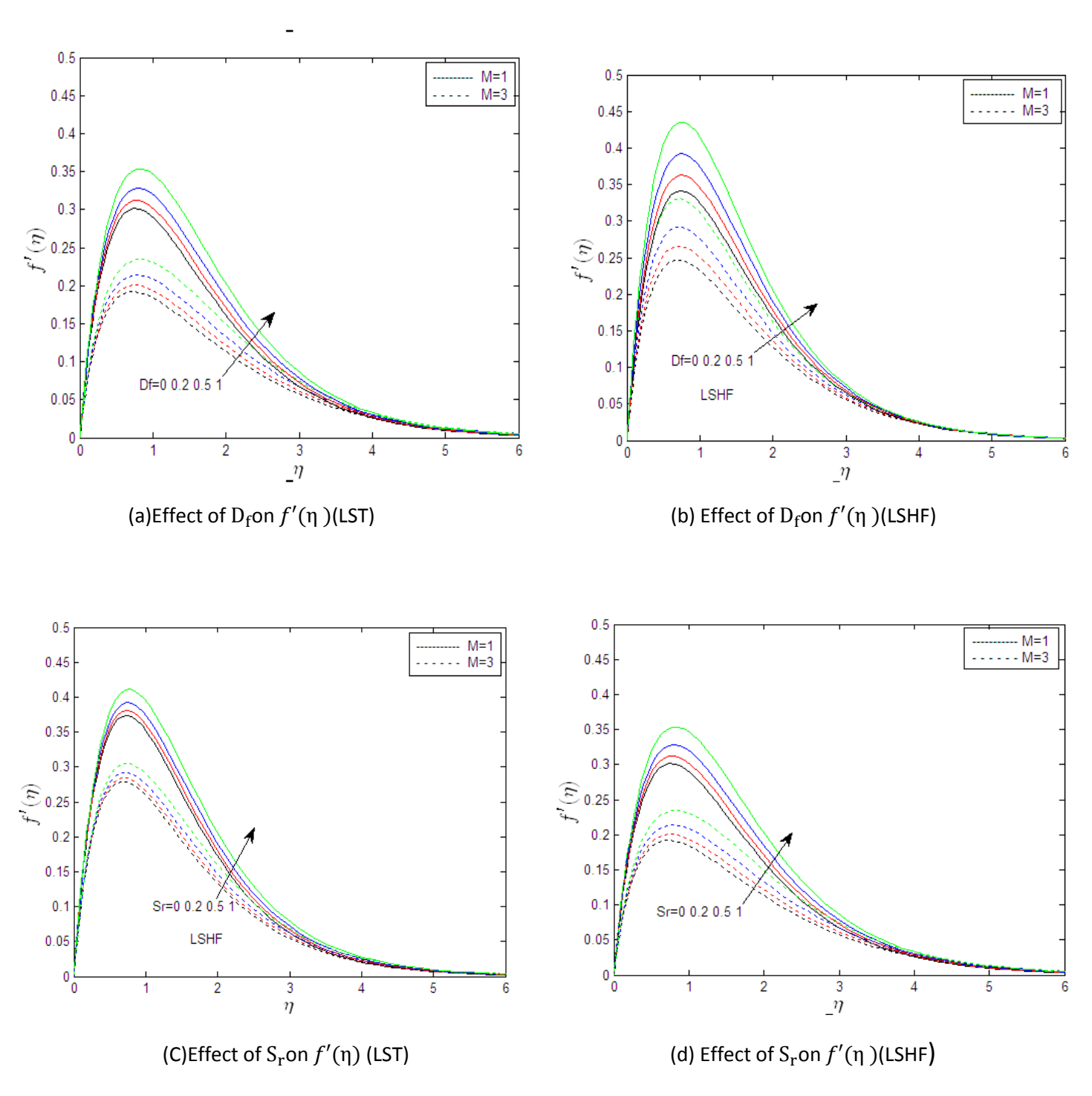


Fig. 5: Variation of axial velocity profiles with Dufour and Soret numbers for different values of magnetic parameter M.

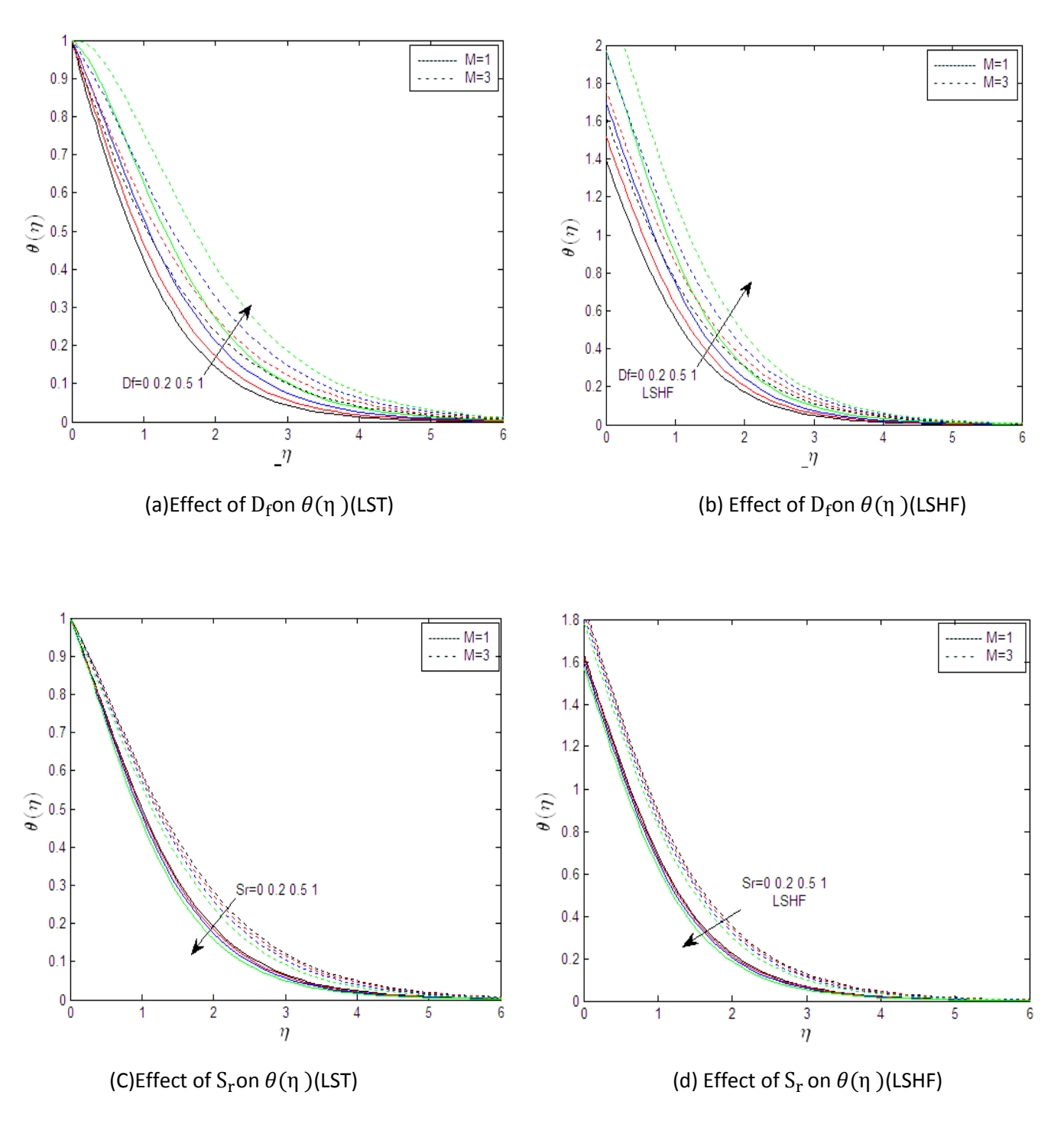


Fig. 6: Variation of temperature profiles with Dufour and Soret numbers for different values of magnetic parameter M.

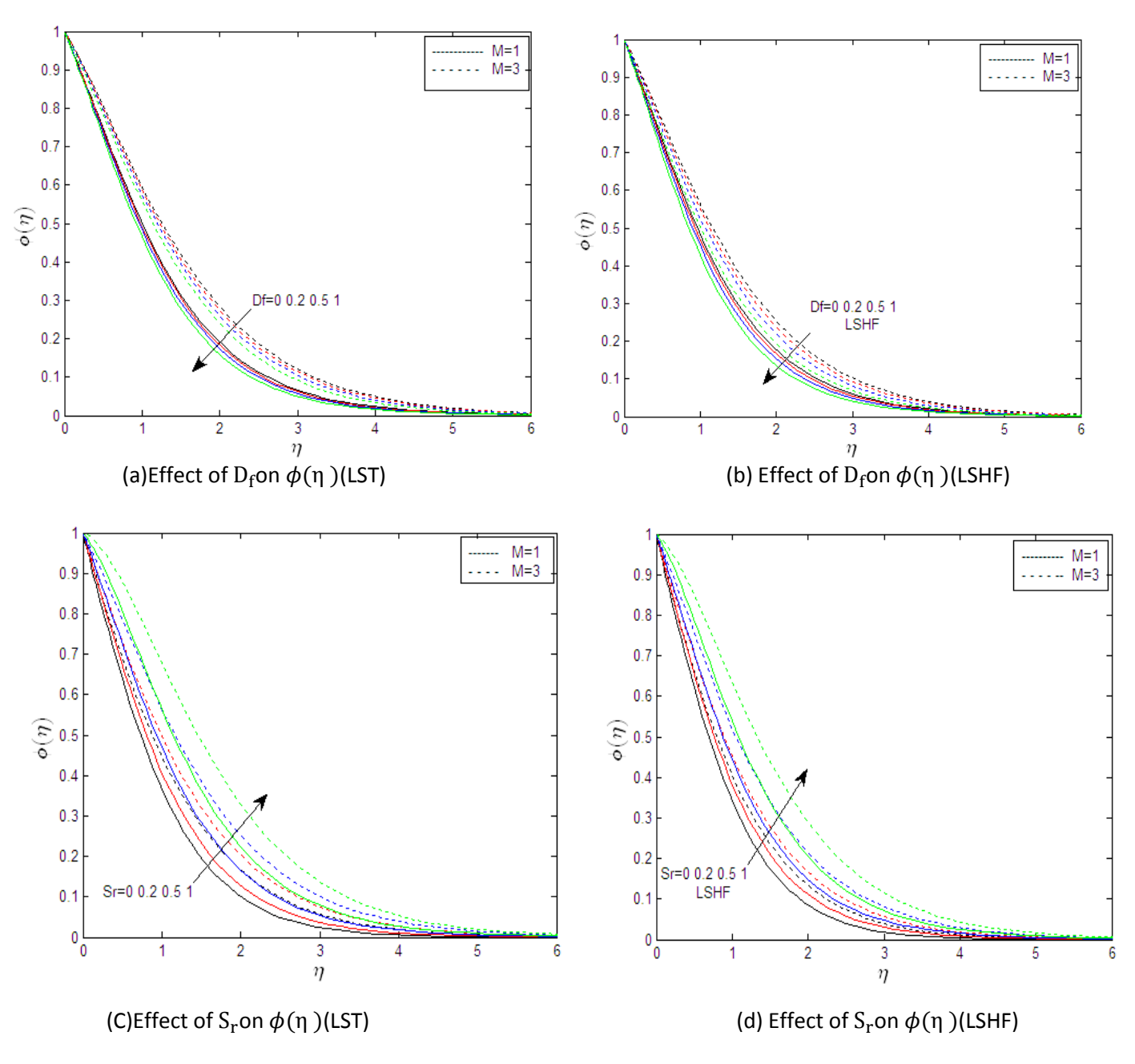


Fig.7: Variation of concentration profiles with Dufour and Soret numbers for different values of magnetic parameter M.

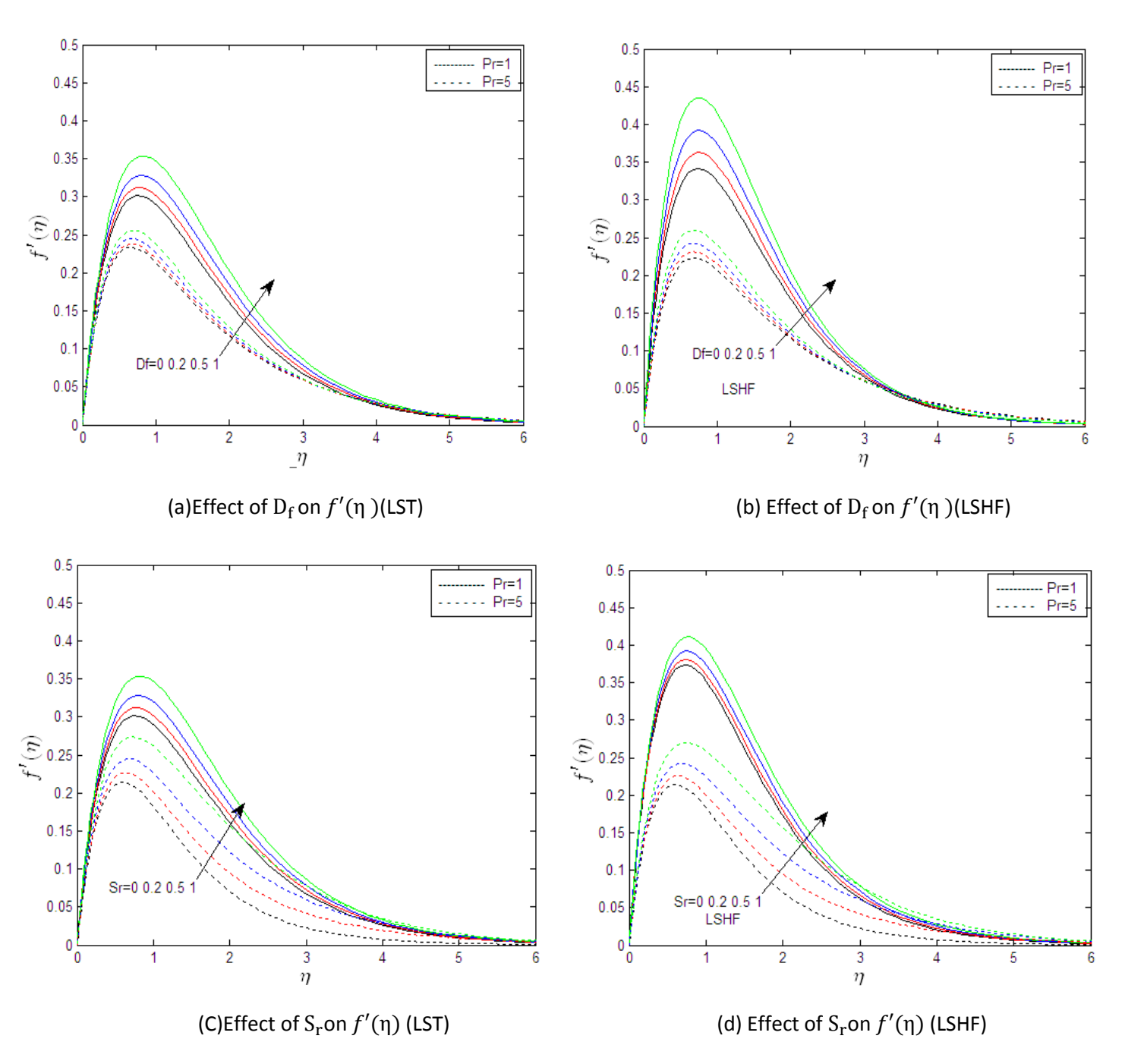


Fig. 8: Variation of axial velocity profiles with Dufour and Soret numbers for different values of Prandtl number Pr.

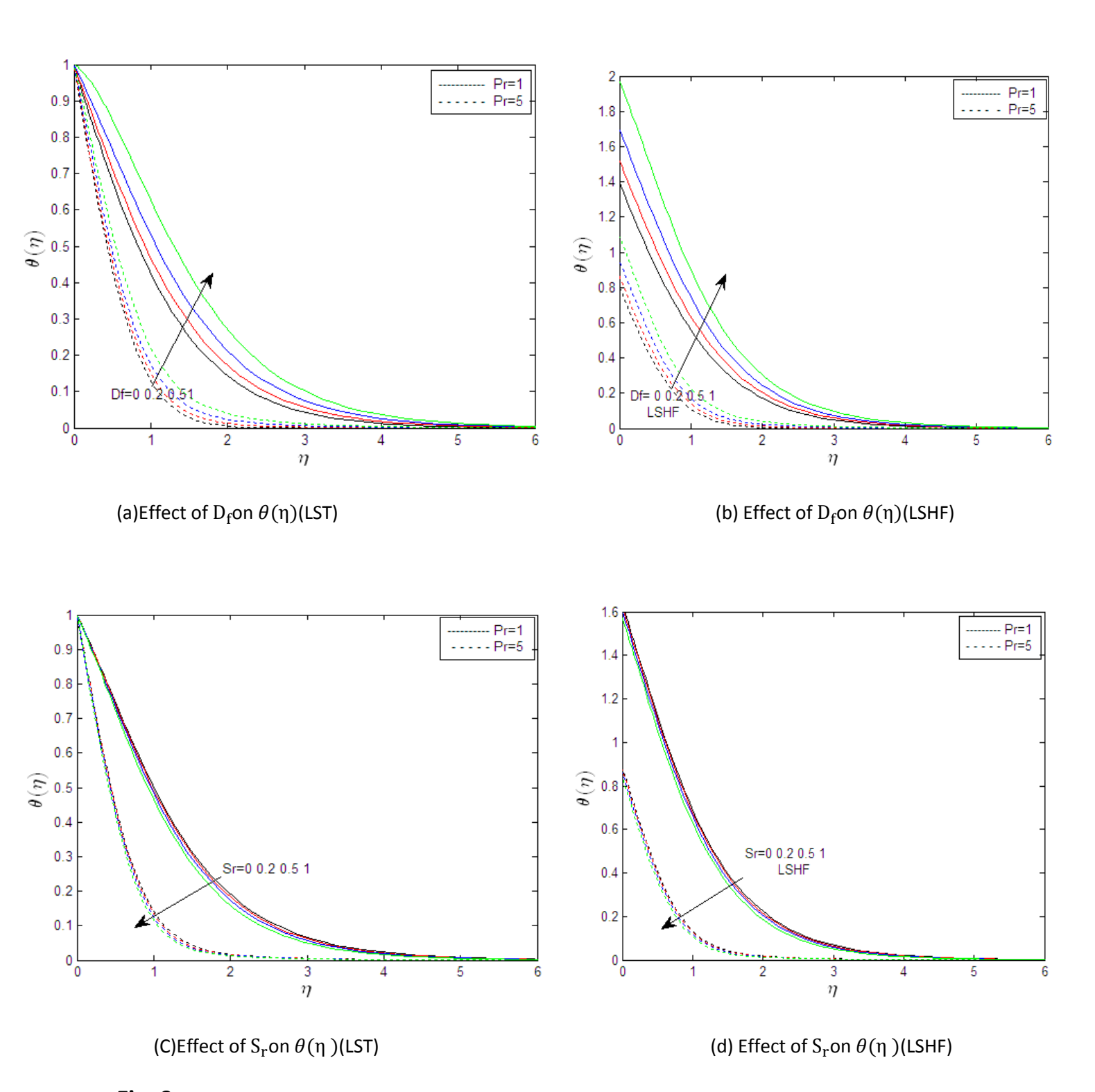


Fig. 9: Variation of temperature profiles with Dufour and Soret numbers for different values of Prandtl number Pr.

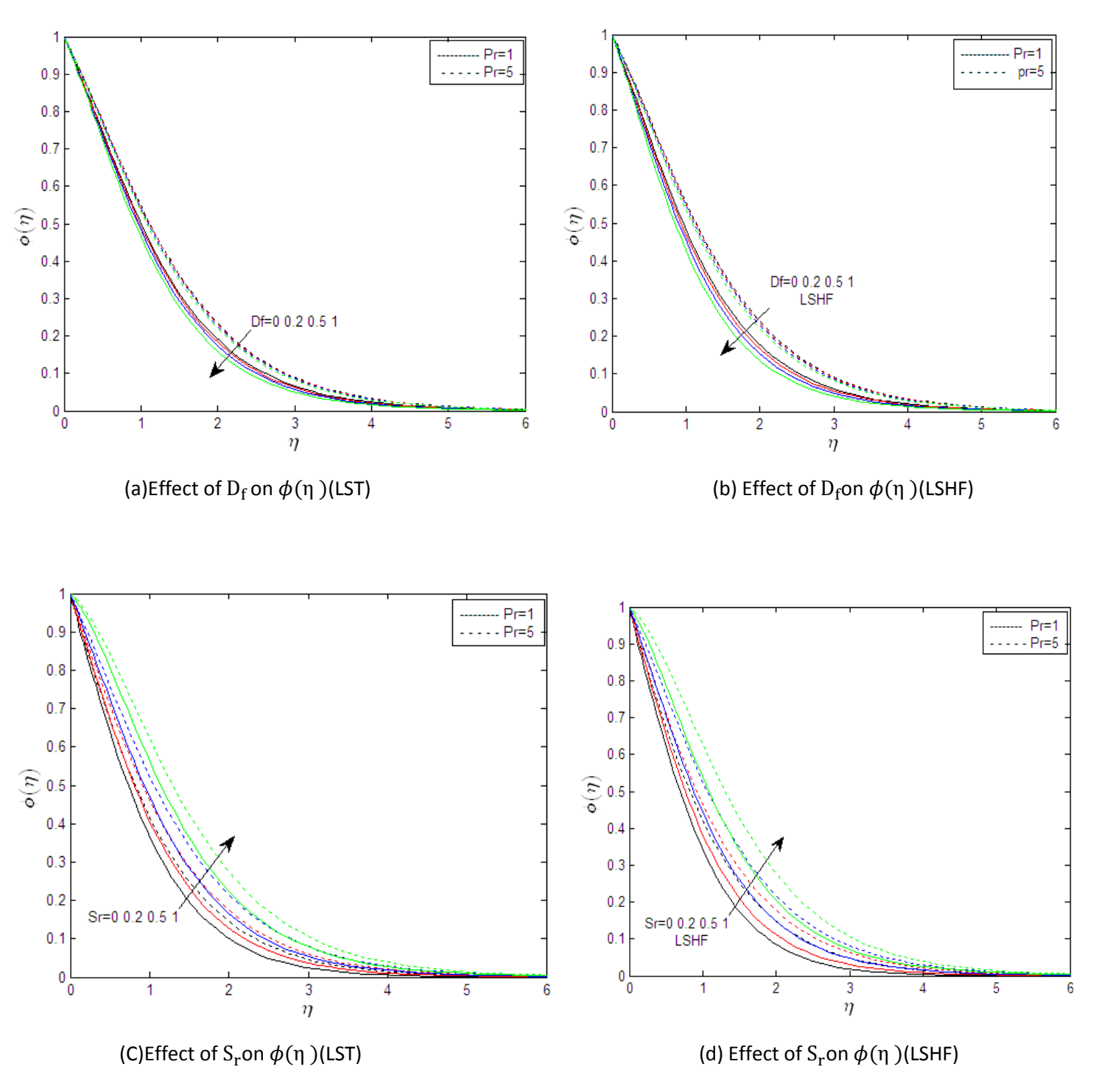


Fig. 10: Variation of concentration profiles with Dufour and Soret numbers for different values of Prandtl number Pr.

Fig.9 shows the temperature distribution for several Dufour and Soret numbers and for two different Prandtl numbers. The effect of the Prandtl number is to reduce the thermal boundary-layer thickness and so reducing the fluid temperature. Qualitatively, the results are in agreement with the findings by

Hassanien et al. [30] and Salama [31]. The effect of Dufour and Soret numbers on the concentration distribution for two different values of Prandtl number is projected in Fig. 10. From the plots it is clear that concentration boundary layer thickness decreases with increasing values of D_f but increases with Sr.

Table1 shows the effect of the of spinning ϵ , Prandtl number Pr and magnetic parameter M on f''(0). The skin friction decreases as magnetic parameter M and Prandtl number Pr increasing, but skin friction increasing as spinning ϵ increasing.

Table 1: Values of f''(0) for double diffusive free convection boundary layer over a spinning cone with linear surface temperature spinning ϵ (LST) and $N = D_f = Sr = 0$.

				•			
		Ece[27]		Narayana		Present	
€	M	f''(0)		f''(0)		f''(0)	
		Pr = 1	Pr = 10	Pr = 1	Pr = 10	Pr = 1	Pr = 10
	0	0.68150212	0.43327726	0.68148313	0.43327500	0.68148350	0.43327824
	1	0.55975901	0.37927751	0.55976132	0.37926796	0.55976166	0.37926856
0	2	0.48678916	0.34866381	0.48680621	0.34865824	0.48680709	0.34865879
	5	0.37090743	0.29345341	0.37090631	0.29345092	0.37098554	0.29345142
	10	0.28500344	0.24343322	0.28490901	0.24340957	0.28517056	0.24343242
	0	0.84650616	0.62601869	0.84648787	0.62601677	0.84648834	0.62601888
	1	0.68547905	0.50300655	0.68548057	0.50299573	0.68548026	0.50299557
0.5	2	0.59002983	0.44721675	0.59004683	0.44721244	0.59004564	0.44721086
	5	0.44274371	0.36247167	0.44261206	0.36247730	0.44281939	0.36246950
	10	0.33709053	0.29437077	0.33701033	0.29435123	0.33725604	0.29437009
	0	1.00196008	0.79828572	1.00194246	0.79828351	1.00194310	0.79828581
	1	0.80819380	0.62583066	0.80819486	0.62582011	0.80819389	0.62581919
1	2	0.69203710	0.54556916	0.69205422	0.54556604	0.69205094	0.54556228
	5	0.51435738	0.43140288	0.51430770	0.43141680	0.51443063	0.43140067
	10	0.38913125	0.34527676	0.38905224	0.34528362	0.38929515	0.34527619
	0	1.29230021	1.10990481	1.29228372	1.10990164	1.29228491	1.10990498
	1	1.04586353	0.86705752	1.04586385	0.86704821	1.04586154	0.86704582
2	2	0.89263261	0.74142462	0.89265068	0.74142554	0.89264320	0.74141738
	5	0.65693141	0.56901873	0.65668889	0.56904825	0.65700000	0.56901605
	10	0.49307448	0.44699636	0.49299748	0.44707960	0.49323504	0.44699601

Table2 shows the effect of the of Prandtl number \Pr and magnetic parameter M of $\theta'(0)$. It is clear that $\theta'(0)$ increasing as Prandtl number \Pr and spinning ϵ increasing, on the other hand side, the $\theta'(0)$ decreases as magnetic parameter M increasing.

Table 2: Values of $\theta'(0)$ for double diffusive free convection boundary layer over a spinning cone with linear surface temperature (LST) and $N=D_f=Sr=0$.

		Ece[27]		Narayana		Present	
ϵ	M	$\theta'(0)$		$\theta'(0)$		$\theta'(0)$	
		Pr = 1	Pr = 10	Pr = 1	Pr = 10	Pr = 1	Pr = 10
	0	0.63886614	1.27552680	0.63885452	1.27551036	0.63885451	1.27552887
	1	0.55869398	1.16243080	0.55869273	1.16241360	0.55869286	1.16242341
0	2	0.50338419	1.09342644	0.50335401	1.09341925	0.50335303	1.09342808
	5	0.40364781	0.95839216	0.40365259	0.95839333	0.40326525	0.95840020
	10	0.32121113	0.82300420	0.32111032	0.82321999	0.31954917	0.82301296
	0	0.67194897	1.47165986	0.67193791	1.47163361	0.67193847	1.47165967
	1	0.58138075	1.27668867	0.58137979	1.27666747	0.58138029	1.27668617
0.5	2	0.51966708	1.17427021	0.51963905	1.17425772	0.51963858	1.17427476
	5	0.41156185	1.00202092	0.41225166	1.00201529	0.41118914	1.00202989
	10	0.32496333	0.84700807	0.32492777	0.84740344	0.32331625	0.84701735
	0	0.70053401	1.60768499	0.70052364	1.60764538	0.70052454	1.60768443
	1	0.60256486	1.37917914	0.60256408	1.37915342	0.60256496	1.37918227
1	2	0.53536409	1.25082089	0.53533784	1.25080261	0.53533788	1.25082871
	5	0.41940005	1.04490075	0.41922547	1.04488853	0.41903739	1.04491128
	10	0.32870765	0.87088877	0.32869140	0.87125491	0.32707561	0.87089863
	0	0.74869559	1.80575019	0.74868659	1.80568032	0.74868825	1.80574944
	1	0.64120157	1.55413661	0.64120160	1.55409454	0.64120327	1.55414680
2	2	0.56516379	1.39136129	0.56514198	1.39132746	0.56514300	1.39137399
	5	0.43485365	1.12833102	0.43474318	1.12830846	0.43451072	1.12834580
	10	0.33617261	0.91826049	0.33601006	0.91834129	0.33457189	0.91827167

Table 3 shows the effect of the of spinning ϵ , Prandtl number Pr and magnetic parameter M of f''(0) in (LSHF). The skin friction decreases as magnetic parameter M and Prandtl number Pr increasing, the skin friction increasing as spinning parameter ϵ increasing.

Table 3: Values of f''(0) for double diffusive free convection boundary layer over a spinning cone with linear surface heat flux (LSHF) and $N=D_f=Sr=0$.

		Ece[27]		Narayana		Present	
ϵ	M	f''(0)		f''(0)		f"(0)	
		Pr = 1	Pr = 10	Pr = 1	Pr = 10	Pr = 1	Pr = 10
							_
							0.7.00.000
	0	1.02528815	0.54034324	1.02528846	0.54034478	1.20380200	0.54034369
	1	0.91396740	0.44894055	0.91397087	0.44894428	1.00100109	0.44894127
0.5	2	0.84705897	0.41308367	0.84706994	0.41308823	0.86657410	0.41308381
	5	0.73956968	0.36208114	0.73941838	0.36209154	0.74358378	0.36208095
	10	0.65637278	0.32257763	0.65665182	0.32257591	0.66213006	0.32257795
	0	1.15592069	0.70152323	1.15592094	0.70152541	1.15992680	0.70152351
	1	1.01801957	0.55685195	1.01802313	0.55685648	1.01801942	0.55685171
1	2	0.93528733	0.49866389	0.93530115	0.49867213	0.93529705	0.49866445
	5	0.80425828	0.42301336	0.80411729	0.42303388	0.80433122	0.42301369
	10	0.70499584	0.36873528	0.70461085	0.36874442	0.70529014	0.36873543
	0	1.40918891	1.00454785	1.40918904	1.00455073	1.40915668	1.00454811
	1	1.22378434	0.77976551	1.22378969	0.77977382	1.22378640	0.77976598
2	2	1.11082540	0.67497148	1.11084268	0.67498553	1.11083392	0.67497161
	5	0.93347602	0.54621284	0.93329155	0.54625325	0.93354713	0.54621396
	10	0.80220839	0.46141862	0.80247495	0.46148692	0.80250032	0.46141938

Table 4 show the effect of the of, Prandtl number Pr, magnetic parameter M and spinning ϵ of temperature. The temperature decreases as magnetic parameter M and Prandtl number Pr increasing, the temperature increasing as spinning ϵ increasing

Table 4: Values of $\theta(0)$ for double diffusive free convection boundary layer over a spinning cone with linear surface heat flux (LSHF) and $N=D_f=Sr=0$.

		Ece[27]		Narayana		Present	
ϵ	M	$\theta(0)$		$\theta(0)$		$\theta(0)$	
		Pr = 1	Pr = 10	Pr = 1	Pr = 10	Pr = 1	Pr = 10
	0	1.38894767	0.71105509	1.38894717	0.71106459	1.40314505	0.71105493
	1	1.52981611	0.81758101	1.52981913	0.81759066	1.50992370	0.81758183
0.5	2	1.64436103	0.87959567	1.64437370	0.87960493	1.65426039	0.87959541
	5	1.90546365	0.99845553	1.90512227	0.99846631	1.91455983	0.99845523
	10	2.21366623	1.12994754	2.18322818	1.12990015	2.19862155	1.12994836
	0	1.35170142	0.64668404	1.35170181	0.64669668	1.35455554	0.64668419
	1	1.49881386	0.75819441	1.49881764	0.75820720	1.49881727	0.75819484
1	2	1.61850659	0.83103877	1.61852096	0.83105287	1.61851869	0.83103941
	5	1.88831408	0.96637696	1.88797632	0.96639248	1.88847081	0.96637629
	10	2.20246048	1.10846998	2.20269483	1.10840939	2.20337841	1.10846934
	0	1.28865472	0.57034570	1.28865664	0.57036447	1.28861016	0.57034594
	1	1.44243526	0.66976417	1.44243956	0.66978298	1.44243628	0.66976409
2	2	1.56988106	0.74969417	1.56989579	0.74971411	1.56989198	0.74969339
	5	1.85491898	0.90700260	1.85444889	0.90702971	1.85507268	0.90700390
	10	2.18032917	1.06718780	2.18074652	1.06713404	2.18124048	1.06718746

Chapter5

Overall conclusions:-

This part of the thesis outlines the main findings in each chapter. We highlight some of the general results that were found and the conclusions that have been drawn from this work.

Chapter 3. To solve the nonlinear equations governed the hydrodynamic and thermal boundary layer flow over a flat plate we used spectral relaxation method developed by Motsa [1]. The solution obtained through the use of the SRM compared with those in the literature review to determine the accuracy and computational efficiency. We also determined the effects of the flow parameters on the fluid properties. Our specific findings were that:

- Both the plate surface temperature and heat transfer coefficients increased with the heat convective parameter.
- As the number of iterations increases, the norm of the residual error of the SRM decreases.
- The SRM takes a few iterations to give accurate.

Chapter 4. We also studied the incompressible Newtonian fluid flow over a vertical down-pointing cone subject to either a linear surface temperature (LST) or the linear surface heat flux (LSHF). The governing equations were solved using the SRM. In both cases LST and LSHF, the effects of the governing parameters have been presented graphically and have also been tabulated. Comparison between the solutions obtained using the SRM, Ece[27] and Narayana[28] showed that the convergence of the SRM was rapid.

- The temperature decreases as the rate of spin increases while the temperature increases with the Dufour parameter.
- The Soret parameter causes a thinning of the thermal boundary layer.
- Increasing the Soret parameter enhances the concentration boundary layer profile in both the LST and LSHF cases.

References

- [1] S. S. Motsa. A new spectral relaxation method for similarity variable nonlinear boundary layerflow systems, *Chemical Engineering Communications*, 201 (2014) 241-256.
- [2] S. S. Motsa and Z. G. Makukula, On spectral relaxation method approach for steady von Karman ow of a Reiner-Rivlinuid with joule heating, viscous dissipation and suction/injection, *Central European Journal of Physics*, 78 (2013) 718-720.
- [3] S. Shateyi, A new numerical approach to MHD ow of a maxwelluid past a vertical stretching sheet in the presence of thermophoresis and chemical reaction, *Boundary Value Problems*, 196 (2013).
- [4] S. Shateyi and O. D. Makinde, Hydromagnetic stagnation-point ow towards a radially stretching convectively heated disk, *Mathematical Problems in Engineering*, (2013), Article ID 616947, 8 pages.
- [5] S. Shateyi and G. T Marewo, A new numerical approach of MHD ow with heat and mass transfer for the UCM uid over a stretching surface in the presence of thermal radiation, *Mathematical Problems in Engineering*, (2013), Article ID 670205, 8 pages.
- [6] S. S. Motsa, P. G. Dlamini and M. Khumalo, Solving Hyperchaotic Systems Using the Spectral Relaxation Method, *Abstract and Applied Mathematics*, 2012:, Article ID 203461, 18 pages doi:10.1155/2012/203461, 2012.97.
- [7] S. S. Motsa, P. G. Dlamini and M. Khumalo, A new multistage spectral relaxation method for solving chaotic initial value systems, *Nonlinear Dynamics*, 72 (2013) 265-283.
- [8] H. S. Nik and P. Rebelo, Multistage Spectral Relaxation Method for Solving the HyperchaoticComplex Systems, *The Scienti_c World Journal*,(2014), Article ID 943293,10 pages.
- [9] P. G. Dlamini, M. Khumalo and S. S. Motsa, A Note on the Multi-stage Spectral Relaxation Method for Chaos Control and Synchronization, *International Journal of Nonlinear Scienceand Numerical Simulation*, 15 (2014) 289-298.
- [10] S. S. Motsa, P. G. Dlamini and M. Khumalo, Spectral Relaxation Method and Spectral Quasilinearization Method for Solving Unsteady Boundary Layer Flow Problems, *Advancesin Mathematical Physics*, (2014), Article ID 341964, 12 pages
- [11] F. Awad, S. S. Motsa and M. Khumalo, Heat and Mass Transfer in Unsteady Rotating Fluid Flow with Binary Chemical Reaction and Activation Energy, *PLOS ONE* 9 (2014): e107622. doi:10.1371/journal.pone.0107622.
- [12] N. A. Haroun, P. Sibanda, S. Mondal and S. S. Motsa, On unsteady MHD mixed convectionin a nanouid due to a stretching/shrinking surface with suction/injection using thespectral relaxation method, *Boundary Value Problems* (2015): 24.

- [13] C. Canuto ,M.Y. Hussaini, A. Quarteroni and T.A. Zang, Spectral Methods in Fluid Dynamics, *Springer-Verlag, Berlin*, 1988.
- [14] B. Fornberg, A Practical Guide to Pseudospectral Methods, *Cambridge University Press*, *Cambridge*, *UK*, 1996.
- [15] L. N. Trefethen, Spectral Methods in MATLAB, SIAM, 2000.
- [16] C. Canuto, M.Y. Hussaini, A. Quarteroni, and T.A. Zang, Spectral Methods in fluid dynamics, Springer-Verlag, Berlin, 1988.
- [17] A.J. Chamkha, A.M. Aly, M.A. Mansour, Similarity solution for unsteady heat and mass transfer from a stretching surface embedded in a porous medium with suction/injection and chemical reaction effects, Chem. Eng. Comm., 197 (2010) 846–858
- [18] B. D. Ganapol, Highly Accurate Solutions of the Blasius and Falkner-Skan Boundary Layer Equations via Convergence Acceleration, arXiv:1006.3888 (June 2010)
- [19] C.Midya, Exact Solutions of Chemically Reactive Solute Distribution in MHD Boundary Layer Flow over a Shrinking Surface, Chin. Phys. Lett. Vol. 29, No. 1 (2012) 014701
- [20] S. Shateyi, S. S. Motsa, Boundary layer flow and double diffusion over an unsteady stretching surface with hall effect, Chemical Engineering Communications, 198:12 (2011)1545–1565
- [21] S.S Motsa, S.Shateyi, Successive Linearisation Analysis of Unsteady Heat and Mass Transfer From a Stretching Surface Embedded in a Porous Medium With Suction/Injection and Thermal Radiation Effects, Can. J. Chem. Eng. 9999:1-13, 2011, DOI 10.1002/cjce.20640
- [22] S. S. Motsa and S. Shateyi, The Effects of Chemical Reaction, Hall, and Ion-Slip Currents on MHD Micropolar Fluid Flow with Thermal Diffusivity Using a Novel Numerical Technique, Journal of Applied Mathematics, vol. 2012, Article ID 689015, 30 pages, 2012. doi:10.1155/2012/689015
- [23] D. Pal, S. Chatterjee, Mixed convection magnetohydrodynamic heat and mass transfer past a stretching surface in a micropolar fluid-saturated porous medium under the influence of Ohmic heating, Soret and Dufour effects, Commun Nonlinear Sci Numer Simulat 16 (2011) 1329–1346
- [24] S. Shateyi, S. S. Motsa, Boundary layer flow and double diffusion over an unsteady stretching surface with Hall effect, Chemical Engineering Communications, 198:12 (2011) 1545–1565

[25] A. Aziz, A similarity solution for laminar thermal boundary layer over a °at plate with a convective surface boundary condition, Commun. *Nonlinear Sci.Numer.Simulat.* 14 (2009) 1064-1068.

[26]O. D. Makinde, Similarity solution of hydromantic heat and mass transfer over a vertical plate with a Convective surface boundary condition, International Journal of the physical Sciences .5(2010) 700-710.

[27] M.C. Ece, Free convection flow over a vertical spinning cone under a magnetic field, Appl. Math. Comput. 179 (2006) 231-242

[28]M.Narayana, F.G. Awad, P. Sibanda, Free magnetohydrodynamic flow and convectionfrom a vertical spinning cone with cross-diffusion effects, *Appl. Math.Modelling* (2012)

[29]M.Q. Al-Odat, T.A. Al-Azab, Influence of chemical reaction on transient MHD free convection over a moving vertical plate, *Emirates J. Engng. Res.* 12 (3)(2007) 15-21.

[30]A.I. Hassanien, A.A. Abdullah, R.S.R Gorla, Flow and heat transfer in a power-law fluid over a nonisothermal stretching sheet, *Math. Comput.Model. 28 (1998) 105-116.*

[31]F.A. Salama, Effect of thermal conductivity on heat transfer for a power-law non-Newtonian fluid over a continuous stretched surface with various injection parameters, *Appl. Math. Mech. 31 (8) (2010) 963-968.*